Article:
Yang, L., Luo, H., Lv, L. et al. (2026) Joint beamforming and beam scheduling in SWIPT for fractionated spacecraft systems. IEEE Journal on Selected Areas in Communications. ISSN: 0733-8716

https://doi.org/10.1109/JSAC.2026.3701682

Joint Beamforming and Beam Scheduling in SWIPT for Fractionated Spacecraft Systems

Long Yang, *Senior Member, IEEE* Hao Luo, Lu Lv, *Member, IEEE* Yuchen Zhou, Xuan Xue, *Member, IEEE* Xiaoli Chu, *Senior Member, IEEE* and Hai Jiang, *Fellow, IEEE*

***Abstract*—Fractionated spacecraft is a novel technology to improve flexibility, robustness, and survivability in future satellite systems by decomposing a traditional spacecraft into multiple functional modules. This paper investigates simultaneous wireless information and power transfer (SWIPT) for a fractionated spacecraft system, where a primary satellite (PS) equipped with a large scale antenna array transmits energy signals to charge multiple energy-constrained miniaturized satellites (MSs) in the near field of the PS, and simultaneously sends information signals to serve ground information receivers (IRs) in the far field of the PS. A joint optimization problem of digital beamforming, analog beamforming, and beam scheduling at the PS is developed to maximize the achievable sum rate of the IRs subject to a requirement on MSs' harvested energy. Due to the highly coupled optimization variables and the binary beam-scheduling variables, the formulated problem is a mixed-integer non-linear programming (MINLP) problem and hence, is difficult to solve. We first develop an alternating optimization algorithm to solve the formulated problem based on the weighted minimum mean-square error method, the manifold optimization method, and the matching theory. To get a low-complexity solution of the formulated problem, we derive the coherence between near- and far-field steering vectors. Then by exploiting the channel coherence, we propose a low-complexity algorithm that transforms the original MINLP problem to a linear programming problem. Numerical results are provided to validate the performance improvement of our proposed algorithms compared to various benchmark schemes, and reveal the practical significance of our developed beamforming and beam scheduling strategies for spectral- and energy-efficient fractionated spacecraft SWIPT.**

***Index Terms*—Fractionated spacecraft, simultaneous wireless information and power transfer, beam scheduling, beamforming, mixed near and far field.**

I. Introduction

Fractionated spacecraft is recognized as a key enabler for future satellite communication systems. Technically, fractionated spacecraft distributes its functionalities, such as data storage, computation, payload, and power generation, into several independent module miniaturized satellites (MSs), sharing those functionalities through a wireless network [1]–[3]. In order to perform information integration, those modules should fly in a cluster. This physically separate yet functionally wireless-linked characteristic makes fractionated spacecrafts significantly unique to other traditional satellite systems. The existing literatures have investigated how to implement a fractionated spacecraft from both hardware and software perspectives [4], [5]. In [4], a wireless transceiver that is specifically designed to meet the mission requirements of fractionated spacecraft system is proposed to make efficient use of limited communications bandwidth over a wide range of spacecraft separation distances and network populations. In [5], a layered software architecture consisting of an operating system, a middleware layer, and component-structured applications is developed to guarantee the stable connectivity among the modules. Main advantages of fractionated spacecraft technology include flexibility to add features later, rapid response, enhanced in-orbit robustness, and lower mission recovery costs [6]–[8]. However, due to the limited on-board power, the operations and lifetime of module MSs are severely restricted. Hence, how to effectively address the energy limitation at an affordable cost is a fundamental issue to achieve sustainable and green satellite networks.

In a fractionated spacecraft system, the MSs need to be charged, and ground users need to be served. Therefore, it is natural to use the simultaneous wireless information and power transfer (SWIPT) technique [9]–[11], in which a primary satellite (PS) transmits energy signals to a number of near-field MS energy receivers, and simultaneously provides communication services to a number of ground information receivers (IRs). SWIPT allows MSs to harvest energy from radio frequency (RF) information signals transmitted by the PS instead of utilizing large-scale solar panels, which significantly reduces the deployment cost of MSs. In the literature, there have been research efforts on SWIPT for fractionated spacecraft systems [12]–[15]. In [12], [13], a system-level feasibility assessment is conducted on the wireless energy transmission problem of the fractionated spacecraft. In [14], a beamforming design is presented as the method to maximize the transmission efficiency while minimizing the interference and power spillover from the sidelobes. In [15], a space simultaneous-information and power-transfer scheme is developed, to extend the lifetime of MSs efficiently and reduce their manufacturing and launching costs.

The aforementioned research works [12]–[15] consider a

This work was supported in part by the National Natural Science Foundation of China under Grants 62271368 and Grant 62371354, in part by the Shaanxi High-Level Talents Special Support Program under Grant H025200001, in part by the Fundamental Research Funds for Central Universities under Grant QTZX26108, in part by the Horizon Europe Research and Innovation Program under grant 101086219, and in part by the UK Engineering and Physical Sciences Research Council grant EP/X038971/1. *(Corresponding author: Lu Lv; Yuchen Zhou).*

Long Yang, Hao Luo, Lu Lv, Yuchen Zhou and Xuan Xue are with the State Key Laboratory of Integrated Services Networks, Xidian University, Xi'an 710071, China (e-mail: lyang@xidian.edu.cn; luohaol23@126.com; {lulv, yuchenzhou9, xuanx}@xidian.edu.cn).

Xiaoli Chu is with the ~~Department of Electronic and Electrical~~ Engineering, The University of Sheffield, U.K. (e-mail: x.chu@sheffield.ac.uk).

Hai Jiang is with the Department of Electrical and Computer Engineering, University of Alberta, Edmonton, AB, Canada T6G 1H9 (e-mail: hai1@ualberta.ca).

small scale antenna array in far-field energy transmission, resulting in very low energy conversion efficiency. However, in fractionated spacecraft scenarios, a module for energy supply and information transmission is usually equipped with an extremely large antenna array (ELAA) to achieve high-directivity beams [16], leading to near-field energy supply for other spacecrafts. In the near field, the ELAA can be exploited to generate focused beams in specific regions, namely beam focusing [17], which can improve the efficiency of energy harvesting (EH) [18]–[20]. Near-field energy supply has been investigated in the literature for traditional SWIPT systems in ground scenarios. A dynamic metasurface antenna aided downlink cellular SWIPT system is investigated in [18], where a base station (BS) transmits energy and information simultaneously to multiple receivers. It is demonstrated that a dynamic metasurface antenna array can help to achieve better rate performance while satisfying a requirement on harvested energy. In [19], a BS uses SWIPT to transmit energy to energy receivers and information bits to IRs. Optimal beamforming is designed, which maximizes the weighted sum energy harvested by all energy receivers while ensuring a minimum information rate requirement of IRs. In [20], it is shown that a single beam can serve multiple energy receivers and IRs, by properly designing the hybrid beamforming of the BS.

The above research efforts [18]–[20] focus on near-field energy and information transmission in ground scenarios. The investigation of satellite near-field energy transmission is still in the early stage. Particularly, consider that a PS, which is an information and energy transmitter, transmits energy signals to a number of near-field MS energy receivers, and simultaneously provides communication services to a number of ground IRs. Since the energy transmissions are in near field, and the information transmissions are in far field, we have a mixed near- and far-field scenario. Mixed-field SWIPT systems have been investigated in [21]–[23] for ground scenarios, in which energy receivers are in near field, and IRs are in far field. The work in [21] considers a reconfigurable intelligent surface (RIS)-assisted SWIPT system, and designs the transmitter's beamforming and the RIS' reflection coefficients. The work in [22] proposes a secure beamforming scheme. The work in [23] designs beam scheduling (i.e., how many beams are assigned?), to maximize the harvested energy at near-field energy receivers. It is shown that, although energy receivers can harvest energy from information beams, in general a dedicated energy beam is still needed.

In this paper, we investigate beamforming and beam scheduling of a PS to serve near-field MSs and far-field IRs. The differences of our work from [21]–[23] are as follows. 1) The work in [21] and [22] assign a beam for each near-field user and each far-field user, and investigate beamforming. However, for our considered mixed-field satellite scenario, based on the existing work [24] and our derivation in Section IV, a beam dedicated for a far-field IR can help the EH of a near-field MS. In addition, a beam dedicated to a near-field MS may generate interference to far-field IRs. According to these two observations, it may not be necessary to assign a dedicated beam for each near-field MS, i.e., a beam scheduling is needed to decide which MSs will be assigned dedicated beams. Therefore, in our work, we investigate both beam scheduling and beamforming of the PS. 2) The work in [23] investigates beam scheduling and power allocation of a BS in serving near-field and far-field ground users. In its beam scheduling, if a user is assigned a beam, the beam direction points directly to the user. We use a different beam scheduling in our mixed-field satellite system. Our major motivation is to adjust the beam direction of a beam for a far-field IR to help EH of near-field MSs. Thus, in our beam scheduling, the PS will decide which MSs/IRs will be assigned beams and to which directions the beams will point. Moreover, the work in [23] uses a successive convex approximation (SCA)-based alternating optimization (AO) algorithm to solve their joint beam-scheduling and power allocation optimization with a computational complexity of $\mathcal{O}(I_{\text{iter}}(K+M)^{3.5})$, where $K+M$ is the total number of receivers and I_{iter} is the number of iterations. In this paper, we propose an AO algorithm that uses a weighted minimum mean-square error (WMMSE) method and the matching theory to achieve better performance than the AO algorithm in [23]. In addition, by exploiting the channel coherence of mixed field to obtain the closed form of beam-scheduling design, we also propose a low-complexity algorithm, which reduces the computation complexity to $\mathcal{O}(I_{\text{iter}}(K+M))$ and also achieves a better performance than the AO algorithm in [23]. 3) The works in [21]–[23] consider ground users, and thus, they use two-dimensional (2D) beams. In our satellite scenario, we need to design three-dimensional (3D) beams, which makes channel modeling and algorithm derivation more complex.

The main contributions of this paper are summarized below.

- We consider a novel SWIPT-enabled fractionated spacecraft system, consisting of an information and energy transmitter PS, K MS energy receivers in the near field, and M IRs in the far field. The PS adopts hybrid beamforming for high-frequency information transmission and energy supply. By jointly optimizing the digital/analog beamforming and the beam scheduling for all the receivers, we formulate an optimization problem to maximize the achievable sum rate of the IRs, subject to a requirement on the MSs' energy demand.
- We propose an AO algorithm to solve the original problem, which optimizes the hybrid beamforming and beam scheduling alternatively. For the hybrid beamforming design, we design a fully digital beamforming by using a weighted minimum mean-square error (WMMSE)-based algorithm. We then derive a closed-form solution for the digital beamforming, and get the analog beamforming by using manifold optimization (MO) to approximate the fully digital beamforming. For the beam scheduling design, a many-to-one matching process is developed to address the challenge of binary variables in the optimization problem.
- We also design a low-complexity algorithm to solve the original problem. We first derive the coherence between the near- and far-field steering vectors by assuming that there is one beam pointing to each IR and MS. Then based on characteristics of the coherence, the beam

scheduling strategy is obtained, and accordingly, the original problem, which is a mixed-integer non-linear programming (MINLP) problem, is transformed to a linear programming (LP) problem, whose optimal solution can be obtained through conventional methods.
- Numerical simulations demonstrate that our proposed algorithms achieve significant performance improvement compared to benchmark schemes. We also have interesting findings: 1) Near- and far-field channel coherence is essential when jointly designing beamforming and beam scheduling in a mixed-field scenario. 2) It is preferable to use far-field information beams for near-field EH, and thus, dedicated energy beams may not be needed in some cases. We also derive cases when energy beams are not needed.

The remainder of this paper is organized as follows. Section II gives the system model for the proposed fractionated spacecraft SWIPT system and the problem formulation. Section III provides the AO algorithm for solving the formulated problem. Section IV derives the coherence between the near- and far-field steering vectors and develops the low-complexity algorithm to solve the formulated problem efficiently. Numerical results are provided in Section V. This paper is concluded with future research directions in Section VI.

Notations: Throughout the paper, we use italic lower-case letters, boldface lower-case letters, and boldface upper-case letters to denote scalars, vectors, and matrices, respectively. The Euclidean norm and the Frobenius norm are denoted by $\|\cdot\|$ and $\|\cdot\|_{\mathrm{F}}$, respectively. $\mathrm{diag}(\mathbf{x})$ means a diagonal matrix whose diagonal elements are from vector $\mathbf{x}$. $\mathcal{CN}(\mu,\sigma^2)$ means circularly symmetric complex Gaussian distribution with mean μ and variance σ^2. $\mathbb{C}^{N\times M}$ means the set of all $N\times M$ matrices. $(\cdot)^T$, $(\cdot)^\dagger$, and $(\cdot)^H$ represent transpose, conjugate, and conjugate transpose operations, respectively. $(\cdot)^\star$ means optimal solution of a problem. $\mathrm{vec}(\mathbf{X})$ means vectorization operation of matrix $\mathbf{X}$. $\Re\{x\}$ means the real part of complex number x. $\circ$ and $\otimes$ denote the Hadamard product and Kronecker product, respectively. $\mathbb{E}(\cdot)$ means expectation operation.

II. System Model and Problem Formulation

A. System Model

We consider a satellite communication system, which is composed of a fractionated spacecraft and M ground IRs, as shown in Fig. 1. Specifically, the fractionated spacecraft contains a PS for energy supply and information transmission, and K MSs for other missions. We assume that the IRs and MSs are all equipped with a single antenna, and the PS is equipped with an N-element uniform linear array (ULA), where $N=2\tilde{N}+1$. The sets of IRs, MSs, and ULA elements are represented as $\mathcal{M}_{\mathrm{IR}}=\{1,\ldots,M\}$, $\mathcal{K}_{\mathrm{MS}}=\{1,\ldots,K\}$, and $\tilde{\mathcal{N}}=\{-\tilde{N},\ldots,\tilde{N}\}$. Due to the limited cost, only the PS is connected to a solar panel, and can transmit information beams to IRs for communication services and simultaneously transmit power beams to MSs for power supply. Each MS has an EH circuit along with a battery for energy storage. All the MSs are located in the near-field region of the ULA, since

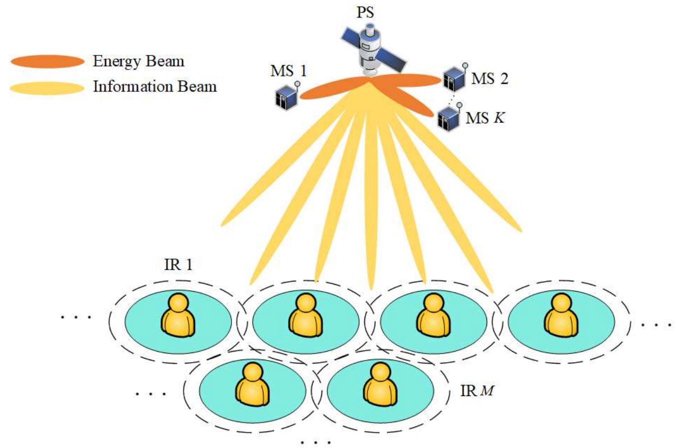

Fig. 1: Fractionated spacecraft enabled SWIPT system.

the distance between the PS and each MS is shorter than the Rayleigh distance $R_{\text{ray}}=\frac{2D^2}{\lambda}$, where $D\approx Nd$ is the antenna aperture of the ULA, d is the antenna spacing, and λ represents the carrier wavelength. On the other hand, due to the extremely large distance between the PS and the ground, IRs lie in the far field of the ULA.

1) Near- and Far-field Channel Models: Here we use the near- and far-field channel models in [23]. The system layout of the PS is shown in Fig. 2. The center of the ULA is located at $(0,0,0)$ in the Cartesian coordinates, and hence the coordinate of the n-th PS antenna is $(0,nd,0)$, with $n\in\{-\tilde{N},\ldots,\tilde{N}\}$. From the near-field spherical wavefront model [25], [26], the distance between MS k and the n-th antenna at the PS is expressed as

$$\begin{aligned} r_k^{(n)} &= \sqrt{r_k^2+n^2d^2-2r_k nd\sin\theta_k\cos\phi_k} \\ &\overset{\text{(i)}}{\approx} r_k - nd\sin\theta_k\cos\phi_k + \frac{n^2d^2(1-\sin^2\theta_k\cos^2\phi_k)}{2r_k}. \end{aligned} \quad (1)$$

In this expression, r_k is the distance between the ULA center and MS k, ϕ_k and θ_k denote the physical azimuth and the physical elevation angle-of-departure (AoD) from the PS center to MS k, respectively, and step (i) is because of the second-order Taylor expansion $\sqrt{1+x}\approx 1+\frac{1}{2}x-\frac{1}{8}x^2$. As such, the free-space near-field channel from the PS to MS k is given as

$$\mathbf{h}_k^{\mathrm{E}} = \sqrt{NG_{\mathrm{R},k}}h_k^{\mathrm{E}}\boldsymbol{b}(\theta_k,\phi_k,r_k), k\in\mathcal{K}_{\mathrm{MS}}, \quad (2)$$

where superscript $(\cdot)^{\mathrm{E}}$ means "energy harvesting", $G_{\mathrm{R},k}$ is the receive antenna gain of MS k, $h_k^E=\frac{\lambda}{4\pi r_k^{(n)}}e^{-j\frac{2\pi}{\lambda}r_k^{(n)}}\approx\frac{\lambda}{4\pi r_k}e^{-j\frac{2\pi}{\lambda}r_k}$ is complex-valued channel gain from any antenna of the PS to MS k,[1] and $\boldsymbol{b}(\theta_k,\phi_k,r_k)$ is the normalized

[1]In the radiative Fresnel region where $r_k > r^{\min} = \max\{\frac{1}{2}\sqrt{\frac{D^3}{\lambda}}, 1.2D\}$, the channel gains from the antennas of the PS to MS k are approximately the same [27]. The condition of the radiative Fresnel region can be easily satisfied. For example, for a PS equipped with $N=512$ antennas, carrier wavelength $\lambda=100$ GHz, and the antenna spacing $d=\frac{\lambda}{2}=0.0015$ m, the boundary of radiative Fresnel region is $r^{\min}=\max\{\frac{1}{2}\sqrt{\frac{D^3}{\lambda}},1.2D\}=3.072$ m, which is significantly smaller than the distance between PS and MS k.

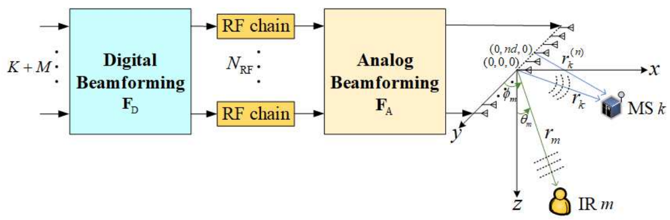

Fig. 2: System layout of the PS.

near-field channel steering vector, expressed as

$$\boldsymbol{b}(\theta_k, \phi_k, r_k) = \frac{1}{\sqrt{N}}[e^{-j\frac{2\pi}{\lambda}(r_k^{(-\tilde{N})} - r_k)}, \ldots, e^{-j\frac{2\pi}{\lambda}(r_k^{(\tilde{N})} - r_k)}]^T. \tag{3}$$

For each IR in the far-field of the PS, similar to (1) and ignoring the second-order term, the distance between IR m and the n-th antenna at the PS is given by

$$r_m^{(n)} = r_m - nd\sin\theta_m\cos\phi_m, \tag{4}$$

where r_m is the distance between the ULA center and IR m, ϕ_m and θ_m denote the physical azimuth AoD and the physical elevation AoD from the PS center to IR m, respectively. Then the far-field free-space channel from the PS to IR m is given by

$$\mathbf{h}_m^{\rm I} = \sqrt{N} h_m^{\rm I} \boldsymbol{a}(\theta_m, \phi_m), m \in \mathcal{M}_{\rm IR}, \tag{5}$$

where superscript $(\cdot)^{\rm I}$ means "information receiving", $h_m^{\rm I} = \frac{\lambda}{4\pi r_m} e^{-j\frac{2\pi}{\lambda} r_m}$ is the complex-valued channel gain from any antenna of the PS to IR m, and $\boldsymbol{a}(\theta_m, \phi_m)$ represents the following normalized far-field channel steering vector

$$\boldsymbol{a}(\theta_m, \phi_m) = \frac{1}{\sqrt{N}}[1, e^{-j\frac{2\pi}{\lambda} d\sin\theta_m\cos\phi_m}, e^{-j\frac{2\pi}{\lambda} 2d\sin\theta_m\cos\phi_m}, \ldots, e^{-j\frac{2\pi}{\lambda} 2\tilde{N} d\sin\theta_m\cos\phi_m}]^T. \tag{6}$$

We assume quasi-static flat fading channels[2], indicating that the channel coefficients are unchanged in one transmission block but vary independently across different transmission blocks. To fully characterize the performance upper bound of the fractionated spacecraft system through beamforming and beam scheduling design, we assume that the PS perfectly knows the channel state information (CSI) of all links, e.g., through channel estimation methods in [29]–[31].

2) Signal Model: The PS utilizes hybrid beamforming architecture to serve the K MSs and M IRs with $N_{\rm RF}$ ($N_{\rm RF} \geq K + M$) RF chains. Letting $x_k^{\rm E}$ denote the energy signal for MS k with $\mathbb{E}(|x_k^{\rm E}|^2) = 1$, and $x_m^{\rm I}$ denote the information signal for IR m with $\mathbb{E}(|x_m^{\rm I}|^2) = 1$, the transmitted signal at the PS is given as

$$\mathbf{x} = \mathbf{F}_{\rm A}\mathbf{F}_{\rm D}\mathbf{A}\mathbf{s}, \tag{7}$$

where $\mathbf{F}_{\rm A} \in \mathbb{C}^{N\times N_{\rm RF}}$ denotes the analog beamforming matrix, $\mathbf{s} = [x_1^{\rm E}, \ldots, x_K^{\rm E}, x_1^{\rm I}, \ldots, x_M^{\rm I}]^T$, $\mathbf{A} = \text{diag}(\alpha_1^{\rm E}, \ldots, \alpha_K^{\rm E}, \alpha_1^{\rm I}, \ldots, \alpha_M^{\rm I})$ is a beam-scheduling matrix with $\alpha_k^{\rm E} = 1$ if a dedicated energy beam is assigned to MS k and $\alpha_k^{\rm E} = 0$ otherwise, and $\alpha_m^{\rm I} = 1$ if a dedicated information beam is assigned to IR m and $\alpha_m^{\rm I} = 0$ otherwise, and $\mathbf{F}_{\rm D} = [\mathbf{f}_{{\rm D},1}^{\rm E}, \ldots, \mathbf{f}_{{\rm D},K}^{\rm E}, \mathbf{f}_{{\rm D},1}^{\rm I}, \ldots, \mathbf{f}_{{\rm D},M}^{\rm I}]^T \in \mathbb{C}^{N_{\rm RF}\times(K+M)}$ denotes the digital beamforming matrix with $\mathbf{f}_{{\rm D},k}^{\rm E} \in \mathbb{C}^{N_{\rm RF}\times 1}$ and $\mathbf{f}_{{\rm D},m}^{\rm I} \in \mathbb{C}^{N_{\rm RF}\times 1}$ representing the digital beamforming vector for MS k and IR m, respectively.

Benefiting from the broadcast characteristic of wireless channels, MS k is capable of harvesting energy not only from its own dedicated energy-bearing signal but also from the energy signals for the other MSs and all the information-bearing signals for IRs. By using a practical non-linear EH model from [32], MS k's harvested energy is denoted as

$$E_k(P_k^{\rm in}) = \frac{\tilde{E}_k(P_k^{\rm in}) - M_k\Omega_k}{1 - \Omega_k}, \forall k \in \mathcal{K}_{\rm MS}, \tag{8}$$

where $\tilde{E}_k(P_k^{\rm in}) = \frac{M_k}{1+\exp(-l_k(P_k^{\rm in} - j_k))}$ is the logistic function with respect to the received RF power $P_k^{\rm in}$, and $\Omega = \frac{1}{1+\exp(l_k j_k)}$. Here, l_k and j_k denote the relevant parameters of the EH circuit for MS k, M_k represents the upper bound of harvested power in MS k, and $P_k^{\rm in}$ is the actual power input at MS k, which is given by

$$P_k^{\rm in} = \alpha_k^{\rm E}|(\mathbf{h}_k^{\rm E})^H \mathbf{F}_{\rm A}\mathbf{f}_{{\rm D},k}^{\rm E} x_k^{\rm E}|^2 + \sum_{i=1, i\neq k}^{K} \alpha_i^{\rm E}|(\mathbf{h}_k^{\rm E})^H \mathbf{F}_{\rm A}\mathbf{f}_{{\rm D},i}^{\rm E} x_i^{\rm E}|^2 + \sum_{m=1}^{M} \alpha_m^{\rm I}|(\mathbf{h}_k^{\rm E})^H \mathbf{F}_{\rm A}\mathbf{f}_{{\rm D},m}^{\rm I} x_m^{\rm I}|^2, \forall k \in \mathcal{K}_{\rm MS}. \tag{9}$$

On the right-hand side of the expression, the first term is the power from the dedicated energy beam for MS k, the second term is the power from the other energy beams, and the last term is the power from all the information beams.

Considering the far-field information transmission, the received signal of IR m is given by

$$y_m = \alpha_m^{\rm I}(\mathbf{h}_m^{\rm I})^H \mathbf{F}_{\rm A}\mathbf{f}_{{\rm D},m}^{\rm I} x_m^{\rm I} + \sum_{i=1, i\neq m}^{M} \alpha_i^{\rm I}(\mathbf{h}_m^{\rm I})^H \mathbf{F}_{\rm A}\mathbf{f}_{{\rm D},i}^{\rm I} x_i^{\rm I} + \sum_{k=1}^{K} \alpha_k^{\rm E}(\mathbf{h}_m^{\rm I})^H \mathbf{F}_{\rm A}\mathbf{f}_{{\rm D},k}^{\rm E} x_k^{\rm E} + n_m^{\rm I}, \forall m \in \mathcal{M}_{\rm IR}, \tag{10}$$

where $n_m^{\rm I} \sim \mathcal{CN}(0, \sigma_m^2)$ is the additive white Gaussian noise at IR m. Therefore, the received signal-to-interference-plus-noise ratio (SINR) of IR m is denoted as (11) on the top of the next page, and the achievable rate of IR m is given by $R_m^{\rm I} = \log_2(1 + \gamma_m^{\rm I})$.

B. Problem Formulation

Our goal is to maximize the system achievable sum rate by jointly optimizing the beam scheduling matrix, digital and analog beamforming matrices, subject to a transmit power

[2]Quasi-static flat fading channel is considered in this paper. Because we consider beamforming and beam scheduling optimization within a single time slot, and the distance between the PS and IRs is extremely large, the movement of the PS in the coherence time will not cause a significant change in the distance between the PS and IRs, which means the channel between PS and IRs can be considered as a constant in the coherence time [28]. Furthermore, in a fractionated spacecraft system, the PS and MSs fly in a cluster with fixed relative positions [7], indicating that the channel between PS and MSs is effectively constant in our considered time slot.

$$\gamma_m^{\mathrm{I}}=\frac{\alpha_m^{\mathrm{I}}|(\mathbf{h}_m^{\mathrm{I}})^H\mathbf{F}_{\mathrm{A}}\mathbf{f}_{\mathrm{D},m}^{\mathrm{I}}|^2}{\sum_{i=1,i\neq m}^{M}\alpha_i^{\mathrm{I}}|(\mathbf{h}_m^{\mathrm{I}})^H\mathbf{F}_{\mathrm{A}}\mathbf{f}_{\mathrm{D},i}^{\mathrm{I}}|^2+\sum_{k=1}^{K}\alpha_k^{\mathrm{E}}|(\mathbf{h}_m^{\mathrm{I}})^H\mathbf{F}_{\mathrm{A}}\mathbf{f}_{\mathrm{D},k}^{\mathrm{E}}|^2+\sigma_m^2},\forall m\in\mathcal{M}_{\mathrm{IR}}, \tag{11}$$

constraint at the PS, a minimum rate requirement of each IR, and a minimum EH constraint at each MS. Accordingly, the optimization problem is formulated as

$$\max_{\mathbf{A},\mathbf{F}_{\mathrm{A}},\mathbf{F}_{\mathrm{D}}}\ \sum_{m=1}^{M}R_m^{\mathrm{I}} \tag{12a}$$
$$\text{s.t.}\quad R_m^{\mathrm{I}}\geq R_{\min,m},\forall m\in\mathcal{M}_{\mathrm{IR}}, \tag{12b}$$
$$E_k(P_k^{\mathrm{in}})\geq E_{\min,k},\forall k\in\mathcal{K}_{\mathrm{MS}}, \tag{12c}$$
$$\sum_{k=1}^{K}\alpha_k^{\mathrm{E}}||\mathbf{F}_{\mathrm{A}}\mathbf{f}_{\mathrm{D},k}^{\mathrm{E}}||^2+\sum_{m=1}^{M}\alpha_m^{\mathrm{I}}||\mathbf{F}_{\mathrm{A}}\mathbf{f}_{\mathrm{D},m}^{\mathrm{I}}||^2\leq P_{\max}, \tag{12d}$$
$$|[\mathbf{F}_{\mathrm{A}}]_{i,j}|=1,\forall i\in\tilde{\mathcal{N}},j\in\{1,\ldots,N_{\mathrm{RF}}\}, \tag{12e}$$
$$\alpha_k^{\mathrm{E}},\alpha_m^{\mathrm{I}}\in\{0,1\},\forall k\in\mathcal{K}_{\mathrm{MS}},m\in\mathcal{M}_{\mathrm{IR}}, \tag{12f}$$

where $P_{\max}$ is the power budget of the PS, $R_{\min,m}$ is the minimum achievable rate required by IR m, $E_{\min,k}$ is the EH requirement for MS k. Constraint (12b) guarantees the quality-of-service (QoS) requirements of the IRs. Constraint (12c) ensures that the energy harvested by MS k is more than its EH requirement $E_{\min,k}$. Constraint (12d) specifies that the total transmit power at the PS is bounded by the transmit power budget $P_{\max}$. Constraint (12e) is the unit-modulus constraint for analog beamforming matrix ($[\mathbf{F}_{\mathrm{A}}]_{i,j}$ means the i-th row and j-th column element of $\mathbf{F}_{\mathrm{A}}$). Constraint (12f) is the binary beam scheduling matrix coefficients for each MS and IR.

There are several challenges in solving problem (12). First, the beam scheduling matrix, digital and analog beamforming matrices are strongly coupled in the objective function (12a) and in constraints (12b)–(12d). Second, the analog beamforming is constrained by a unit modulus, which is essentially non-convex. Third, problem (12) is a MINLP problem due to the binary beam-scheduling variables in (12f), and hence is NP-hard. Thus, it is generally challenging to optimally solve Problem (12).

To solve Problem (12), we will first propose an AO algorithm in Section III, and develop a low-complexity algorithm in Section IV.

Remark 1: Both the proposed AO algorithm and low-complexity algorithm can solve this MINLP problem (12) effectively, and they strike different tradeoffs between performance and computational complexity. The AO algorithm is a general method that divides the original problem (12) into multiple subproblems and optimizes them alternately. It does not need any specific structural assumptions of the problem or the channel model, making it applicable to general scenarios and achieve a good enough performance. On the other hand, the low-complexity algorithm utilizes the inherent channel coherence of the mixed field to obtain a closed form of beam-scheduling design, and thus, the original MINLP problem (12) can be further simplified to an LP problem, which can be solved with significantly lower computational complexity. However, due to the fixed beam directions, the low-complexity algorithm has a lower achievable sum rate than that of the AO algorithm, which will be discussed in Section V.

III. AO Algorithm Design

This section develops an effective AO algorithm to solve problem (12). Each AO iteration has two steps. First, we fix a beam scheduling matrix, and utilize a WMMSE algorithm to design the full-digital beamforming. Then, we derive the digital beamforming in closed form, and obtain the analog beamforming using the MO algorithm. Next we fix the PS beamforming, and exploit the matching theory to optimize the beam scheduling matrix. The AO algorithm converges after a number of iterations.

Section III-A and Section III-B will detail the two steps for an iteration (say, the $(q+1)$-th iteration).

A. Hybrid Beamforming Design in the $(q+1)$-th iteration

At the $(q+1)$-th iteration, based on $\mathbf{F}_{\mathrm{A}}^{(q)}$, $\mathbf{F}_{\mathrm{D}}^{(q)}$, and $\mathbf{A}^{(q)}$ that are obtained in the q-th iteration, we will get the hybrid beamforming design, as follows. Note that superscript $(\cdot)^{(q)}$ represents a notation in the q-th iteration of AO.

1) Full-Digital Beamforming Design: Define $\mathbf{F}=\mathbf{F}_{\mathrm{A}}\mathbf{F}_{\mathrm{D}}=[\mathbf{f}_1^{\mathrm{E}},\ldots,\mathbf{f}_K^{\mathrm{E}},\mathbf{f}_1^{\mathrm{I}},\ldots,\mathbf{f}_M^{\mathrm{I}}]\in\mathbb{C}^{N\times(K+M)}$ as the fully digital beamforming matrix at the PS. Accordingly, problem (12) is reformulated as

$$\max_{\mathbf{F}}\ \sum_{m=1}^{M}\tilde{R}_m^{\mathrm{I}} \tag{13a}$$
$$\text{s.t.}\quad \tilde{R}_m^{\mathrm{I}}\geq R_{\min,m},\forall m\in\mathcal{M}_{\mathrm{IR}} \tag{13b}$$
$$E_k(\bar{P}_k^{\mathrm{in}})\geq E_{\min,k},\forall k\in\mathcal{K}_{\mathrm{MS}}, \tag{13c}$$
$$\sum_{k=1}^{K}\alpha_k^{\mathrm{E}}||\mathbf{f}_k^{\mathrm{E}}||^2+\sum_{m=1}^{M}\alpha_m^{\mathrm{I}}||\mathbf{f}_m^{\mathrm{I}}||^2\leq P_{\max}, \tag{13d}$$

where $\tilde{R}_m^{\mathrm{I}}$ and $\bar{P}_k^{\mathrm{in}}$ are given as (14) and (15) on the top of next page, respectively, with $\tilde{\mathbf{h}}_i^{\mathrm{I}}=\alpha_i^{\mathrm{I}}\mathbf{h}_i^{\mathrm{I}},\forall i\in\mathcal{M}_{\mathrm{IR}}$ and $\tilde{\mathbf{h}}_j^{\mathrm{E}}=\alpha_j^{\mathrm{E}}\mathbf{h}_j^{\mathrm{E}},\forall j\in\mathcal{K}_{\mathrm{MS}}$.

By employing the WMMSE algorithm, we transform $\tilde{R}_m^{\mathrm{I}}$ in (13a) and (13b) into a more tractable form. Specifically, the signal y_m is estimated by the corresponding equalizer u_m as $\tilde{y}_m=u_my_m$. Then, the mean-square-error (MSE) for y_m can be written as

$$e_m=\mathbb{E}(|y_m-\tilde{y}_m|^2)=|u_m|^2\sigma_m^2-2\Re\{u_m(\tilde{\mathbf{h}}_m^{\mathrm{I}})^H\mathbf{f}_m^{\mathrm{I}}\}+|u_m|^2\left(\sum_{i=1}^{M}|(\tilde{\mathbf{h}}_i^{\mathrm{I}})^H\mathbf{f}_i^{\mathrm{I}}|^2+\sum_{k=1}^{K}|(\tilde{\mathbf{h}}_k^{\mathrm{E}})^H\mathbf{f}_k^{\mathrm{E}}|^2\right)+1. \tag{16}$$

We introduce a positive weight v_m for IR m. As such, problem (13) can be equivalently reformulated as [34]

$$\min_{\mathbf{F},\{v_m\},\{u_m\}}\ \sum_{m=1}^{M}v_me_m-\log_2|v_m| \tag{17a}$$

$$\tilde{R}^{\mathrm{I}}_m = \log_2\left(1+\frac{|(\tilde{\mathbf{h}}^{\mathrm{I}}_m)^H\mathbf{f}^{\mathrm{I}}_m|^2}{\sum_{i=1,i\neq m}^{M}|(\tilde{\mathbf{h}}^{\mathrm{I}}_m)^H\mathbf{f}^{\mathrm{I}}_i|^2+\sum_{k=1}^{K}|(\tilde{\mathbf{h}}^{\mathrm{I}}_m)^H\mathbf{f}^{\mathrm{E}}_k|^2+\sigma_m^2}\right), \forall m\in\mathcal{M}_{\mathrm{IR}}, \tag{14}$$

$$\bar{P}^{\mathrm{in}}_k = |(\tilde{\mathbf{h}}^{\mathrm{E}}_k)^H\mathbf{f}^{\mathrm{E}}_k|^2+\sum_{i=1,i\neq k}^{K}|(\tilde{\mathbf{h}}^{\mathrm{E}}_k)^H\mathbf{f}^{\mathrm{E}}_i|^2+\sum_{m=1}^{M}|(\tilde{\mathbf{h}}^{\mathrm{E}}_k)^H\mathbf{f}^{\mathrm{I}}_m|^2, \forall k\in\mathcal{K}_{\mathrm{MS}}. \tag{15}$$

$$\begin{aligned}\text{s.t.}\quad & (13c),(13d),\\ & \log_2|v_m|-v_m e_m+1\geq R_{\min,m}, \forall m\in\mathcal{M}_{\mathrm{IR}}. \end{aligned}\tag{17b}$$

For problem (17), the optimal values of u_m and v_m can be represented as [34]

$$v_m^\star = 1+\frac{|(\tilde{\mathbf{h}}^{\mathrm{I}}_m)^H\mathbf{f}^{\mathrm{I}}_m|^2}{\sum_{i\neq m}^{M}|(\tilde{\mathbf{h}}^{\mathrm{I}}_m)^H\mathbf{f}^{\mathrm{I}}_i|^2+\sum_{k=1}^{K}|(\tilde{\mathbf{h}}^{\mathrm{I}}_m)^H\mathbf{f}^{\mathrm{E}}_k|^2+\sigma_m^2}, \tag{18}$$

$$u_m^\star = \frac{(\tilde{\mathbf{h}}^{\mathrm{I}}_m)^H\mathbf{f}^{\mathrm{I}}_m}{\sum_{i\neq m}^{M}|(\tilde{\mathbf{h}}^{\mathrm{I}}_m)^H\mathbf{f}^{\mathrm{I}}_i|^2+\sum_{k=1}^{K}|(\tilde{\mathbf{h}}^{\mathrm{I}}_m)^H\mathbf{f}^{\mathrm{E}}_k|^2+\sigma_m^2}. \tag{19}$$

For the EH constraint (13c), by using the inverse function of $E_k(\bar{P}^{\mathrm{in}}_k)$, we get an equivalent form of (13c) as

$$\begin{aligned}\bar{P}^{\mathrm{in}}_k &\geq \bar{P}^{\mathrm{in}}_k(E_{\min,k})\\ &= j_k-\frac{1}{l_k}\ln\left(\frac{M_k}{(1-\Omega_k)E_{\min,k}+M_k\Omega_k}-1\right), \forall k. \end{aligned}\tag{20}$$

Substituting the expression of $\bar{P}^{\mathrm{in}}_k$ (i.e., (15)) into (20), we obtain the following equivalent form of constraint (13c)

$$\sum_{i=1}^{K}|(\tilde{\mathbf{h}}^{\mathrm{E}}_k)^H\mathbf{f}^{\mathrm{E}}_i|^2+\sum_{m=1}^{M}|(\tilde{\mathbf{h}}^{\mathrm{E}}_k)^H\mathbf{f}^{\mathrm{I}}_m|^2\geq \bar{P}^{\mathrm{in}}_k(E_{\min,k}), \forall k. \tag{21}$$

Subsequently, by deriving the first-order Taylor expansion at the given points $(\mathbf{f}^{\mathrm{E}}_i)^{(q)}$ and $(\mathbf{f}^{\mathrm{I}}_m)^{(q)}$, we have

$$\begin{aligned}|(\tilde{\mathbf{h}}^{\mathrm{E}}_k)^H\mathbf{f}^{\mathrm{E}}_i|^2 &= (\mathbf{f}^{\mathrm{E}}_i)^H\mathbf{H}_k\mathbf{f}^{\mathrm{E}}_i \geq 2\Re\{(\mathbf{f}^{\mathrm{E}}_i)^{(q)H}\mathbf{H}_k\mathbf{f}^{\mathrm{E}}_i\}\\ &\quad -(\mathbf{f}^{\mathrm{E}}_i)^{(q)H}\mathbf{H}_k(\mathbf{f}^{\mathrm{E}}_i)^{(q)} \triangleq G(\mathbf{f}^{\mathrm{E}}_i,\tilde{\mathbf{h}}^{\mathrm{E}}_k), \end{aligned}\tag{22}$$

where $\mathbf{H}_k=\tilde{\mathbf{h}}^{\mathrm{E}}_k(\tilde{\mathbf{h}}^{\mathrm{E}}_k)^H$, and $(\mathbf{f}^{\mathrm{E}}_i)^{(q)}$ is the solutions of $\mathbf{f}^{\mathrm{E}}_i$ at the q-th iteration. Similarly, the lower bound of $|(\tilde{\mathbf{h}}^{\mathrm{E}}_k)^H\mathbf{f}^{\mathrm{I}}_m|^2$ is obtained as $G(\mathbf{f}^{\mathrm{I}}_m,\tilde{\mathbf{h}}^{\mathrm{E}}_k)$. With $G(\mathbf{f}^{\mathrm{I}}_m,\tilde{\mathbf{h}}^{\mathrm{E}}_k)$ and $G(\mathbf{f}^{\mathrm{E}}_i,\tilde{\mathbf{h}}^{\mathrm{E}}_k)$, constraint (21) is transformed into the following convex form

$$\sum_{i=1}^{K}G(\mathbf{f}^{\mathrm{E}}_i,\tilde{\mathbf{h}}^{\mathrm{E}}_k)+\sum_{m=1}^{M}G(\mathbf{f}^{\mathrm{I}}_m,\tilde{\mathbf{h}}^{\mathrm{E}}_k)\geq \bar{P}^{\mathrm{in}}_k(E_{\min,k}), \forall k. \tag{23}$$

Therefore, the full-digital beamforming optimization problem (13) is transformed as

$$\begin{aligned}\min_{\mathbf{F}}\ & \sum_{m=1}^{M} v_m^\star e_m|_{u_m=u_m^\star}-\log_2|v_m^\star| \\ \text{s.t.}\ & (13d),(17b),(23), \end{aligned}\tag{24}$$

which is a convex Quadratically Constrained Quadratic Program (QCQP) problem. An optimal solution of the QCQP problem can be obtained by using interior-point methods.

2) Hybrid Beamforming Design: Based on the obtained full-digital beamforming design, next we get our digital beamforming design and analog beamforming design.

To approximate the performance of the full-digital beamforming $\mathbf{F}^\star$ obtained in problem (24), we formulate the following hybrid beamforming design problem

$$\begin{aligned}\min_{\mathbf{F}_{\mathrm{A}},\mathbf{F}_{\mathrm{D}}}\ & \|\mathbf{F}^\star-\mathbf{F}_{\mathrm{A}}\mathbf{F}_{\mathrm{D}}\|_{\mathrm{F}}^2 \\ \text{s.t.}\ & (12e). \end{aligned}\tag{25}$$

Owing to the inherent coupling between the analog and digital beamforming, an alternating minimization approach is developed to optimize them [33].

- *Digital beamforming design:* Given $\mathbf{F}_{\mathrm{A}}$, problem (25) can be rewritten as

$$\min_{\mathbf{F}_{\mathrm{D}}} ||\mathbf{F}^\star-\mathbf{F}_{\mathrm{A}}\mathbf{F}_{\mathrm{D}}||_{\mathrm{F}}^2. \tag{26}$$

  Optimal solution of the problem in (26) is given as

$$\mathbf{F}_{\mathrm{D}}^\star = \left(\mathbf{F}_{\mathrm{A}}^H\mathbf{F}_{\mathrm{A}}\right)^{-1}\mathbf{F}_{\mathrm{A}}^H\mathbf{F}^\star. \tag{27}$$

- *Analog beamforming design:* Given $\mathbf{F}_{\mathrm{D}}$, optimization problem (25) is simplified as

$$\begin{aligned}\min_{\mathbf{F}_{\mathrm{A}}}\ & ||\mathbf{F}^\star-\mathbf{F}_{\mathrm{A}}\mathbf{F}_{\mathrm{D}}||_{\mathrm{F}}^2 \\ \text{s.t.}\ & (12e), \end{aligned}\tag{28}$$

  which has an equivalent form

$$\begin{aligned}\min_{\mathbf{F}_{\mathrm{A}}}\ & e(\mathrm{vec}(\mathbf{F}_{\mathrm{A}}))\triangleq||\mathrm{vec}(\mathbf{F}^\star)-\left(\mathbf{F}_{\mathrm{D}}^T\otimes\mathbf{I}_{N_{\mathrm{RF}}}\right)\mathrm{vec}(\mathbf{F}_{\mathrm{A}})||^2 \\ \text{s.t.}\ & (12e). \end{aligned}\tag{29}$$

  A MO algorithm is used to solve the problem in (III-A2), which consists of three steps.

  a) *Computation of Riemannian Gradient:* The Riemannian gradient $\mathrm{grad}_{\mathrm{vec}(\mathbf{F}_{\mathrm{A}})}e(\mathrm{vec}(\mathbf{F}_{\mathrm{A}}))$, which is obtained by orthogonally projecting the Euclidean gradient $\bigtriangledown_{\mathrm{vec}(\mathbf{F}_{\mathrm{A}})}e(\mathrm{vec}(\mathbf{F}_{\mathrm{A}}))$ onto the tangent space, can be expressed as

$$\begin{aligned}\mathrm{grad}_{\mathrm{vec}(\mathbf{F}_{\mathrm{A}})}e(\mathrm{vec}(\mathbf{F}_{\mathrm{A}})) &= \bigtriangledown_{\mathrm{vec}(\mathbf{F}_{\mathrm{A}})}e(\mathrm{vec}(\mathbf{F}_{\mathrm{A}}))-\mathrm{vec}(\mathbf{F}_{\mathrm{A}})\\ &\quad\circ\Re\{\bigtriangledown_{\mathrm{vec}(\mathbf{F}_{\mathrm{A}})}e(\mathrm{vec}(\mathbf{F}_{\mathrm{A}}))\circ\mathrm{vec}(\mathbf{F}_{\mathrm{A}})^\dagger\}, \end{aligned}\tag{30}$$

  where the $\bigtriangledown_{\mathrm{vec}(\mathbf{F}_{\mathrm{A}})}e(\mathrm{vec}(\mathbf{F}_{\mathrm{A}}))$ is given by (31) on the top of next page.

  b) *Finding Search Direction:* The search direction is given as

$$\mathbf{d} = -\mathrm{grad}_{\mathrm{vec}(\mathbf{F}_{\mathrm{A}})}e(\mathrm{vec}(\mathbf{F}_{\mathrm{A}}))+\omega\mathbb{T}(\bar{\mathbf{d}}). \tag{32}$$

  Here ω denotes the conjugate gradient update parameter, $\bar{\mathbf{d}}$ denotes the search direction, and $\mathbb{T}(\bar{\mathbf{d}})=\bar{\mathbf{d}}-\Re\{\mathbf{d}\,\circ$

$$\nabla_{\mathrm{vec}(\mathbf{F}_{\mathrm{A}})} e(\mathrm{vec}(\mathbf{F}_{\mathrm{A}})) = 2\big(\mathbf{F}_{\mathrm{D}}^{T} \otimes \mathbf{I}_{N_{\mathrm{RF}}}\big)^{H} \big(\mathbf{F}_{\mathrm{D}}^{T} \otimes \mathbf{I}_{N_{\mathrm{RF}}}\big)\mathrm{vec}(\mathbf{F}_{\mathrm{A}}) - 2\big(\mathbf{F}_{\mathrm{D}}^{T} \otimes \mathbf{I}_{N_{\mathrm{RF}}}\big)^{H}\mathrm{vec}(\mathbf{F}^{\star}). \tag{31}$$

$\mathrm{vec}(\mathbf{F}_{\mathrm{A}})^{\dagger}\} \circ \mathrm{vec}(\mathbf{F}_{\mathrm{A}})$.

c) *Retraction:* The retraction maps the point $\mathrm{vec}(\mathbf{F}_{\mathrm{A}})$ on the tangent space back to the complex circle manifold to obtain the next iteration solution. Mathematically, it is defined as

$$[\mathrm{vec}(\mathbf{F}_{\mathrm{A}})]_n \triangleq \frac{[\mathrm{vec}(\bar{\mathbf{F}}_{\mathrm{A}}) + \tau\mathbf{d}]_n}{|[\mathrm{vec}(\bar{\mathbf{F}}_{\mathrm{A}}) + \tau\mathbf{d}]_n|}, \tag{33}$$

where $[\cdot]_n$ denotes the n-th element of a vector, a tilde above a notation refers to the previous iteration, and τ denotes the step size.

By using the alternating minimization approach, we can get digital beamforming design and analog beamforming design. Now we should make sure that constraints (12b)–(12d) are satisfied with the obtained digital beamforming design and analog beamforming design. We assume that the number of RF chains is at least twice the number of receivers (MSs and IRs). With this assumption, it is guaranteed that the hybrid beamforming matrices can perfectly approximate any full-digital beamforming design [35], and thus constraints (12b)–(12d) are satisfied. When the above assumption is not satisfied, we can introduce small margins, denoted by ϱ, $R_{\varrho,m}$, and $E_{\varrho,k}$ when we design the full-digital beamforming matrix so that we have constraints $\sum_{k=1}^{K}\alpha_k^{\mathrm{E}}||\mathbf{F}_k^{\mathrm{E}}||^2+\sum_{m=1}^{M}\alpha_m^{\mathrm{I}}||\mathbf{F}_m^{\mathrm{I}}||^2 \leq P_{\max}+\varrho$, $\tilde{R}_m^{\mathrm{I}} \geq R_{\min,m}+R_{\varrho,m}$, and $E_k(\bar{P}_k^{\mathrm{in}}) \geq E_{\min,k}+E_{\varrho,k}$, respectively, which are more stringent than the constraints (12b)–(12d). By taking appropriate margins, the obtained digital beamforming design and analog beamforming design may make constraints (12b)–(12d) satisfied.

B. *Beam Scheduling Design in the $(q+1)$-th Iteration*

Given $\mathbf{F}_{\mathrm{A}}^{(q+1)}$ and $\mathbf{F}_{\mathrm{D}}^{(q+1)}$ obtained in the $(q+1)$-th iteration, next we design $\mathbf{A}^{(q+1)}$, i.e., we determine whether or not a receiver (MS or IR) needs a dedicated beam. If a receiver has a dedicated beam, we say that the receiver has beam-scheduling status 1; otherwise, the receiver has beam-scheduling status 0. Therefore, the beam scheduling design is actually a many-to-one matching: we match each user to a status in $\mathbb{L}=\{0,1\}$.

To mathematically characterize the matching, denote $\mathbb{Z}$ as the set of $Z=K+M$ receivers (say, K MSs and M IRs). We have the following definition.

Definition 1: A many-to-one matching Φ is a matching between the receiver set $\mathbb{Z}$ to the status set $\mathbb{L}$. Denoting $\Phi(z)$ ($z \in \mathbb{Z}$) as the status that receiver z is matched to and $\Phi(l)$ ($l \in \mathbb{L}$) as the set of receivers that are matched to status l, we have the following properties

(a) $\Phi(z) \in \mathbb{L}$;
(b) $\Phi(l) \subseteq \mathbb{Z}$;
(c) $|\Phi(z)|=1, |\Phi(l)| \leq Z$;
(d) $\Phi(z)=l \iff z \in \Phi(l)$.

In Definition 1, property (a) and property (b) indicate that each receiver only matches with one status and each status can be matched with a subset of receivers, property (c) means that at most Z receivers can be assigned to each state, and property (d) indicates that z and l are matched with each other.

Since information beams can be used to charge MSs, the preference (i.e., the preferred status) of each receiver may be affected by other receivers' status. Hence, we conclude that beam-scheduling problem is a many-to-one matching problem with externalities [36].

Based on the above definition, the solution of the many-to-one matching problem can be obtained by the following three steps: 1) Initialize the matching unit satisfying Definition 1; 2) Check each of the Z receivers. For checking of a receiver (say, receiver z), if changing the status of receiver z and applying the corresponding beamforming strategies achieves a higher system achievable sum rate, we change the status of receiver z. 3) Repeat step 2) until the achievable sum rate cannot be increased by changing status of any receiver.

C. *Overall Algorithm*

With the above results, we derive an AO algorithm by optimizing the PS beamforming and beam scheduling matrix alternatively until convergence, where each iteration uses the solution obtained in the previous iteration as an initial point. The developed AO algorithm is summarized in Algorithm 1.

Convergence: The convergence of the AO Algorithm is proved as follows. Denote the achievable sum rate at the end of the q-th iteration as $\mathcal{F}(\mathbf{F}_{\mathrm{A}}^{(q)},\mathbf{F}_{\mathrm{D}}^{(q)},\Phi^{(q)})$. Then at the $(q+1)$-th iteration, we first fix $\Phi^{(q)}$ and solve problem (24) to obtain the optimal beamforming design $\mathbf{F}_{\mathrm{A}}^{(q+1)},\mathbf{F}_{\mathrm{D}}^{(q+1)}$, resulting in a non-decreasing achievable sum rate, i.e., $\mathcal{F}(\mathbf{F}_{\mathrm{A}}^{(q)},\mathbf{F}_{\mathrm{D}}^{(q)},\Phi^{(q)}) \leq \mathcal{F}(\mathbf{F}_{\mathrm{A}}^{(q+1)},\mathbf{F}_{\mathrm{D}}^{(q+1)},\Phi^{(q)})$. Then in beam scheduling design of the $(q+1)$-th iteration, we change the beam scheduling decision for a MS/IR if this can increase the achievable sum rate. Thus, the achievable sum rate is non-decreasing after the beam scheduling design, i.e., $\mathcal{F}(\mathbf{F}_{\mathrm{A}}^{(q+1)},\mathbf{F}_{\mathrm{D}}^{(q+1)},\Phi^{(q)}) \leq \mathcal{F}(\mathbf{F}_{\mathrm{A}}^{(q+1)},\mathbf{F}_{\mathrm{D}}^{(q+1)},\Phi^{(q+1)})$. Thus, overall, the achievable sum rate is non-decreasing from an iteration to the next. On the other hand, the system has an upper bound on its achievable sum rate as the PS' transmit power is limited. Therefore, the AO algorithm is guaranteed to converge.

Complexity: The computational complexity of Algorithm 1 is calculated below. Since the calculations of Step 4 and Step 6 are given by closed-form solutions, the computational complexity of Algorithm 1 is greatly determined by Step 5 and Step 7. In Step 5, the complexity for solving Problem (24) is in the order of $\mathcal{O}((K+M)N^3)$ [37]. In Step 7, the complexity for solving Problem (28) using an MO algorithm is given by $\mathcal{O}((K+M)N^2)$ [38]. Denote the numbers of iterations for the WMMSE method, MO method, matching theory and the overall AO algorithm are I_{W}, I_{MO}, I_{M}, and I_{AO}, the total computational complexity of Algorithm 1 is $\mathcal{O}(I_{\mathrm{AO}}I_{\mathrm{M}}(I_{\mathrm{W}}((K+M)N^3)+I_{\mathrm{MO}}((K+M)N^2)))$.

Algorithm 1 AO for Solving (12)

Initialize variable $\{\mathbf{F}_{\mathrm{A}}^{(0)}, \mathbf{F}_{\mathrm{D}}^{(0)}, \mathbf{A}^{(0)}, \Phi^{(0)}\}$, iteration index $q = 0$, and threshold ε.
repeat
  repeat
    Update v_m and u_m in (18) and (19).
    Update $\mathbf{F}^{(q+1)}$ by solving problem (24) with fixed $\mathbf{A}^{(q)}$ and $\Phi^{(q)}$.
    Update $\mathbf{F}_{\mathrm{D}}^{(q+1)}$ in (27) with fixed $\mathbf{F}^{(q+1)}$ and $\mathbf{F}_{\mathrm{A}}^{(q)}$.
    Update $\mathbf{F}_{\mathrm{A}}^{(q+1)}$ by solving problem (28) with fixed $\mathbf{F}_{\mathrm{D}}^{(q+1)}$ and $\mathbf{F}^{(q+1)}$.
  until the fractional decrease of (24) is below ε.
  Update $\mathbf{A}^{(q+1)}$ by changing matching configuration $\Phi^{(q)}$.
  $q = q + 1$.
until $\Phi^{(q+1)}$ is a stable matching.

IV. Low-complexity Algorithm Design

In this section, we design a low-complexity algorithm to solve problem (12). Specifically, we first reformulate the problem and then derive the coherence between near- and far-field steering vectors. By exploiting the characteristics of the derived coherence, the original problem is transformed to an LP problem to optimize the power allocation.

A. Problem Reformulation

Denote $\tilde{\mathbf{F}} = [\tilde{\mathbf{f}}_1^{\mathrm{E}}, \ldots, \tilde{\mathbf{f}}_K^{\mathrm{E}}, \tilde{\mathbf{f}}_1^{\mathrm{I}}, \ldots, \tilde{\mathbf{f}}_M^{\mathrm{I}}] \in \mathbb{C}^{N\times(K+M)}$ and $\mathbf{P} = \mathrm{diag}(\sqrt{P_1^{\mathrm{E}}}, \ldots, \sqrt{P_K^{\mathrm{E}}}, \sqrt{P_1^{\mathrm{I}}}, \ldots, \sqrt{P_M^{\mathrm{I}}})$ satisfy $\mathbf{P}\tilde{\mathbf{F}} = \mathbf{F}_{\mathrm{A}}\mathbf{F}_{\mathrm{D}}$. Thereafter, let $\tilde{\mathbf{f}}_k^{\mathrm{E}} = \boldsymbol{b}(\theta_k, \phi_k, r_k), \forall k \in \mathcal{K}_{\mathrm{MS}}$ and $\tilde{\mathbf{f}}_m^{\mathrm{I}} = \boldsymbol{a}(\theta_m, \phi_m), \forall m \in \mathcal{M}_{\mathrm{IR}}$, we can rewrite the power input at MS k and the achievable rate of IR m as (34) and (35) on the top of the next page, where $g_k^{\mathrm{E}} = NG_{\mathrm{R},k}|h_k^{\mathrm{E}}|^2$ and $g_m^{\mathrm{I}} = N|h_m^{\mathrm{I}}|^2$. Hence, problem (12) can be reformulated as

$$\max_{\mathbf{A},\mathbf{P}} \sum_{m=1}^{M} \tilde{R}_m^{\mathrm{I}} \tag{36a}$$

$$\text{s.t.} \quad \tilde{R}_m^{\mathrm{I}} \geq R_{\min,m}, \forall m \in \mathcal{M}_{\mathrm{IR}} \tag{36b}$$

$$E_k(\tilde{P}_k^{\mathrm{in}}) \geq E_{\min,k}, \forall k \in \mathcal{K}_{\mathrm{MS}}, \tag{36c}$$

$$\sum_{k=1}^{K} \alpha_k^{\mathrm{E}} P_k^{\mathrm{E}} + \sum_{m=1}^{M} \alpha_m^{\mathrm{I}} P_m^{\mathrm{I}} \leq P_{\max}, \tag{36d}$$

$$\alpha_k^{\mathrm{E}}, \alpha_m^{\mathrm{I}} \in \{0,1\}, \forall k \in \mathcal{K}_{\mathrm{MS}}, m \in \mathcal{M}_{\mathrm{IR}}, \tag{36e}$$

which is non-convex due to the binary variables (36e) and the non-convex objective function. Thus, it is still challenging to solve problem (36). In the following part of this section, we first provide some useful insights for the beam scheduling matrix $\mathbf{A}$, and then transform problem (36) to an LP problem, which can be solved efficiently.

B. Coherence Evaluation Between IRs and MSs

We derive the coherence between the channels of IRs and MSs, so as to shed useful insights for the beam-scheduling design. The coherence between two near-field steering vectors located at (θ_1, ϕ_1, r_1) and (θ_2, ϕ_2, r_2) in the polar coordinate system can be expressed as follows

$$\begin{aligned} f(\theta_1, \theta_2, \phi_1, \phi_2, r_1, r_2) &= |\boldsymbol{b}(\theta_1, \phi_1, r_1)^H \boldsymbol{b}(\theta_2, \phi_2, r_2)| \\ &= \left| \frac{1}{N} \sum_{n=(1-N)/2}^{(N-1)/2} \exp\{j\kappa(r_1^{(n)} - r_2^{(n)})\} \right| \\ &\approx \left| \frac{1}{N} \sum_{n=(1-N)/2}^{(N-1)/2} \exp\{j\kappa\big(nd(\sin\theta_2\cos\phi_2 - \sin\theta_1\cos\phi_1) \right. \\ &\quad \left. + \frac{n^2 d^2}{2}\big(\frac{1-\sin^2\theta_1\cos^2\phi_1}{r_1} - \frac{1-\sin^2\theta_2\cos^2\phi_2}{r_2}\big)\big)\} \right|, \end{aligned} \tag{37}$$

where $\kappa \triangleq \frac{2\pi}{\lambda}$. Although the above expression is derived for two near-field steering vectors, the expression can also characterize the near- and far-field coherence, since the near-field channel model is a general version of the far-field channel model. The phase of each term in the summation of (37) has two components. The first component is the linear phase $nd(\sin\theta_2\cos\phi_2 - \sin\theta_1\cos\phi_1)$ related to the angular difference. The second component is the quadratic phase $\frac{n^2d^2}{2}\big(\frac{1-\sin^2\theta_1\cos^2\phi_1}{r_1} - \frac{1-\sin^2\theta_2\cos^2\phi_2}{r_2}\big)$, which depends on both the angle and the distance. Similar to [39], we will develop an angular beam-scheduling method based on the linear phase component, and develop a distance beam-scheduling method based on the quadratic phase component.

1) Azimuth angle Beam-scheduling Method: To design the azimuth angle beam-scheduling method, we are supposed to focus on the linear phase component $nd(\sin\theta_2\cos\phi_2 - \sin\theta_1\cos\phi_1)$, which only depends on the angular difference. Therefore, we need to first eliminate the influence of the quadratic phase component $\frac{n^2d^2}{2}\big(\frac{1-\sin^2\theta_1\cos^2\phi_1}{r_1} - \frac{1-\sin^2\theta_2\cos^2\phi_2}{r_2}\big)$ in the steering vectors coherence (37). In the polar coordinate, denote a surface as $\frac{1-\sin^2\theta\cos^2\phi}{r} = \frac{1}{\delta}$, where δ is a constant. For any two points located at (θ_1, ϕ_1, r_1) and (θ_2, ϕ_2, r_2) on the surface in the polar coordinate, their locations satisfy $\frac{n^2d^2}{2}\big(\frac{1-\sin^2\theta_1\cos^2\phi_1}{r_1} - \frac{1-\sin^2\theta_2\cos^2\phi_2}{r_2}\big) = \frac{1}{\delta}$, and then it is obvious that the quadratic phase component $\frac{n^2d^2}{2}\big(\frac{1-\sin^2\theta_1\cos^2\phi_1}{r_1} - \frac{1-\sin^2\theta_2\cos^2\phi_2}{r_2}\big) = 0$, and thus it can be removed from (37). Then, at the same elevation angle (i.e., $\theta_1 = \theta_2 = \theta$), the linear phase component $nd(\sin\theta_2\cos\phi_2 - \sin\theta_1\cos\phi_1)$ is equivalent to $nd\sin\theta(\cos\phi_2 - \cos\phi_1)$, and hence the coherence $f(\theta_1, \theta_2, \phi_1, \phi_2, r_1, r_2) = f(\theta, \theta, \phi_1, \phi_2, r_1, r_2)$ only depends on the azimuth difference $\cos\phi_2 - \cos\phi_1$, and then we rewrite the coherence $f(\theta, \theta, \phi_1, \phi_2, r_1, r_2)$ as follows

$$\begin{aligned} f(\theta, \theta, \phi_1, \phi_2, r_1, r_2) &= \left| \frac{1}{N} \sum_{n=(1-N)/2}^{(N-1)/2} e^{j\kappa nd\sin\theta(\cos\phi_2 - \cos\phi_1)} \right| \\ &\overset{\text{(ii)}}{=} \frac{1}{N} \left| \frac{e^{-j\frac{N-1}{2}\psi}\big(1 - e^{jN\psi}\big)}{1 - e^{j\psi}} \right| \\ &= \frac{1}{N} \left| \frac{-2j\sin\frac{N\psi}{2} e^{-j\frac{N-1}{2}\psi} e^{\frac{jN\psi}{2}}}{-2j\sin\frac{\psi}{2} e^{\frac{j\psi}{2}}} \right| = \frac{1}{N} \left| \frac{\sin\frac{N\psi}{2}}{\sin\frac{\psi}{2}} \right| \end{aligned}$$

$$\tilde{P}_k^{\text{in}} = \alpha_k^{\text{E}} P_k^{\text{E}} g_k^{\text{E}} + \sum_{i=1, i\neq k}^{K} \alpha_i^{\text{E}} P_i^{\text{E}} g_k^{\text{E}} |\boldsymbol{b}^H(\theta_k, \phi_k, r_k)\boldsymbol{b}(\theta_i, \phi_i, r_i)|^2 + \sum_{m=1}^{M} \alpha_m^{\text{I}} P_m^{\text{I}} g_k^{\text{E}} |\boldsymbol{b}^H(\theta_k, \phi_k, r_k)\boldsymbol{a}(\theta_m, \phi_m)|^2, \quad (34)$$

$$\tilde{R}_m^{\text{I}} = \log_2\left(1 + \frac{\alpha_m^{\text{I}} P_m^{\text{I}} g_m^{\text{I}}}{\sum_{i=1, i\neq m}^{M} \alpha_i^{\text{I}} P_i^{\text{I}} g_m^{\text{I}} |\boldsymbol{a}^H(\theta_m, \phi_m)\boldsymbol{a}(\theta_i, \phi_i)|^2 + \sum_{k=1}^{K} \alpha_k^{\text{E}} P_k^{\text{E}} g_m^{\text{I}} |\boldsymbol{a}^H(\theta_m, \phi_m)\boldsymbol{b}(\theta_k, \phi_k, r_k)|^2 + \sigma_m^2}\right). \quad (35)$$

$$\overset{\text{(iii)}}{\approx} \left|\frac{\sin\frac{N\psi}{2}}{\frac{N\psi}{2}}\right| = \left|\text{sinc}(\frac{N\psi}{2})\right|, \quad (38)$$

where step (ii) arises because of the equivalent substitution $\kappa d \sin\theta(\cos\phi_2 - \cos\phi_1) = \psi$, and step (iii) results from the fact that $\sin\frac{\psi}{2} \approx \frac{\psi}{2}$ when $\frac{\psi}{2} \to 0$. Moreover, the numerical results of function $|\text{sinc}(\cdot)|$ are widely known. Therefore, in order to maximally improve the coherence, i.e., let $f(\theta,\theta,\phi_1,\phi_2,r_1,r_2) \approx \left|\text{sinc}(\frac{N\psi}{2})\right|$ higher than a desired threshold Γ, we can calculate the range of azimuth angles that have a strong correlation with any given point (θ_0,ϕ_0,r_0) at the same elevation angle on the surface $\frac{1-\sin^2\theta\cos^2\phi}{r} = \frac{1}{\delta}$. The range of azimuth angles is defined as the *azimuth beam-width*. For example, if we desire the threshold $\Gamma = 0.5$, it can be solved from $\left|\text{sinc}(\frac{N\psi}{2})\right| \geq 0.5$ that $\left|\frac{N\psi}{2}\right| \leq 1.8955$. Substituting the equation $\kappa d \sin\theta_0(\cos\phi - \cos\phi_0) = \psi$ into $\left|\frac{N\psi}{2}\right| \leq 1.8955$ yields the angle range $[\arccos(\frac{1.8955\lambda}{N\pi d \sin\theta_0} + \cos\phi_0), \arccos(\frac{-1.8955\lambda}{N\pi d\sin\theta_0} + \cos\phi_0)]$ and the azimuth beam-width $\text{A-BW}_{\text{3dB}} = \arccos(\frac{-1.8955\lambda}{N\pi d \sin\theta_0} + \cos\phi_0) - \arccos(\frac{1.8955\lambda}{N\pi d\sin\theta_0} + \cos\phi_0)$.

According to the above observation, the points that are in the obtained azimuth angle range have a strong coherence with the given point (θ_0,ϕ_0,r_0), indicating that the beam directed towards the given point has strong energy in the azimuth beam-width. Therefore, we have the following lemma for our azimuth angle beam-scheduling method.

Lemma 1: For MS $(\theta_k,\phi_k,r_k), \forall k \in \mathcal{K}_{\text{MS}}$, if $\exists m \in \mathcal{M}_{\text{IR}}$ satisfying $\theta_k = \theta_m$, and $\phi_k \in [\arccos(\frac{\phi_\Delta\lambda}{N\pi d\sin\theta_m} + \cos\phi_m), \arccos(\frac{-\phi_\Delta\lambda}{N\pi d\sin\theta_m} + \cos\phi_m)]$, where ϕ_Δ is the solution of inequality $\left|\text{sinc}(\frac{N\psi}{2})\right| \geq \Gamma$, the beam-scheduling matrix element of MS k is given by $\alpha_k^{\text{E}} = 0$; otherwise, the beam-scheduling matrix element of MS k is given by $\alpha_k^{\text{E}} = 1$.

Proof: Please refer to Appendix A. ■

Remark 2: Lemma 1 shows the fact that an MS can harvest sufficient energy from an information beam of a far-field IR to maintain its functionality, when the MS is in the azimuth beam-width of the IR. On the contrary, if the MS is not in azimuth beam-width of any far-field IR, a dedicated energy beam is needed to provide energy for the MS.

Lemma 2: For each IR in the far-field region, a dedicated information-bearing beam must be needed to provide communication services, i.e., $\alpha_m^{\text{I}} = 1, \forall m \in \mathcal{M}_{\text{IR}}$.

Proof: We prove Lemma 2 by contradiction. If $\exists m \in \mathcal{M}_{\text{IR}}$ satisfying $\alpha_m^{\text{I}} = 0$, the achievable rate of IR m is 0 since $\gamma_m^{\text{I}}|_{\alpha_m^{\text{I}}=0} = 0$ holds, as observed from (11). This fact indicates that there is no reliable communication service for IR m, which contradicts the QoS requirement constraint (12b). This completes the proof. ■

2) Elevation angle Beam-scheduling Method: Since the elevation angle θ is always coupled with the azimuth angle ϕ in (37), the impact of elevation angle on (37) is exactly the same as that of azimuth angle. As a result, by using the similar derivation to that utilized in Section IV-B1, we can calculate the range of elevation angles that have a strong correlation with any given point (θ_0,ϕ_0,r_0) at the same azimuth angle on the surface $\frac{1-\sin^2\theta\cos^2\phi}{r} = \frac{1}{\delta'}$ (δ' is a constant). The range of elevation angles is defined as the *elevation beam-width*. Similarly, based on the 3dB criterion, i.e., $\Gamma = 0.5$, we have $\left|\frac{N\psi'}{2}\right| \leq 1.8955$, and then substituting the equation $\kappa d\cos\phi_0(\sin\theta - \sin\theta_0) = \psi'$ into $\left|\frac{N\psi'}{2}\right| \leq 1.8955$ yields the elevation beam-width $\text{E-BW}_{\text{3dB}} = \arcsin(\frac{1.8955\lambda}{N\pi d\cos\phi_0} + \sin\theta_0) - \arcsin(\frac{-1.8955\lambda}{N\pi d\cos\phi_0} + \sin\theta_0)$. Based on the above derivation, we have the following lemma for elevation angle beam-scheduling method.

Lemma 3: For MS $(\theta_k,\phi_k,r_k), \forall k \in \mathcal{K}_{\text{MS}}$, if $\exists m \in \mathcal{M}_{\text{IR}}$ satisfying $\phi_k = \phi_m$, and $\theta_k \in [\arcsin(\frac{-\theta_\Delta\lambda}{N\pi d\cos\phi_m} + \sin\theta_m), \arcsin(\frac{\theta_\Delta\lambda}{N\pi d\cos\phi_m} + \sin\theta_m)]$, where θ_Δ is the solution of inequality $\left|\text{sinc}(\frac{N\psi'}{2})\right| \geq \Gamma$, the beam-scheduling matrix element of MS k is given by $\alpha_k^{\text{E}} = 0$; otherwise, the beam-scheduling matrix element of MS k is given by $\alpha_k^{\text{E}} = 1$.

Proof: This lemma can be proved using the similar steps given in Appendix A. ■

3) Distance Beam-scheduling Method: For any two points located at the same azimuth angle ϕ and elevation angle θ, i.e., $\phi_1 = \phi_2 = \phi$, and $\theta_1 = \theta_2 = \theta$, the first linear phase component $nd(\sin\theta_2\cos\phi_2 - \sin\theta_1\cos\phi_1)$ can be removed from (37). Then, the coherence $f(\theta_1,\theta_2,\phi_1,\phi_2,r_1,r_2) = f(\theta,\theta,\phi,\phi,r_1,r_2)$ depends on the second quadratic phase component $\frac{n^2d^2}{2}(\frac{1-\sin^2\theta_1\cos^2\phi_1}{r_1} - \frac{1-\sin^2\theta_2\cos^2\phi_2}{r_2}) = \frac{n^2d^2(1-\sin^2\theta\cos^2\phi)}{2}(\frac{1}{r_1} - \frac{1}{r_2})$, which relies on the distance-related terms $\frac{1}{r_1}$ and $\frac{1}{r_2}$. Based on the above observation, we have the following lemma related to the coherence of the steering vectors in the distance domain.

Lemma 4: For any given point (θ_0,ϕ_0,r_0), a largest interval $[r_{\min}, r_{\max}]$ can be found from the same azimuth angle ϕ_0 and the same elevation angle θ_0, which makes $\forall r \in [r_{\min}, r_{\max}]$ satisfy $\frac{1}{N}\left|\boldsymbol{b}(\theta_0,\phi_0,r_0)^H\boldsymbol{b}(\theta_0,\phi_0,r)\right| \geq \Gamma$. Then, the depth of beam focusing can be defined as $\Xi \triangleq r_{\max} - r_{\min}$. Specifically, if Ξ is calculated based on the 3dB criterion, i.e., $\Gamma = 0.5$, the 3 dB depth of focus is given by

$$\Xi_{\text{3dB}} = \begin{cases} \frac{2r_0^2 r_{\text{DF}}}{r_{\text{DF}}^2 - r_0^2}, & r_0 < r_{\text{DF}}, \\ \infty, & r_0 \geq r_{\text{DF}}, \end{cases} \quad (39)$$

where $r_{\text{DF}} \triangleq \frac{N^2d^2(1-\sin^2\theta_0\cos^2\phi_0)}{2\lambda\eta_{\text{3dB}}^2}$ and $\eta_{\text{3dB}} = 1.6$.

Proof: Please refer to Appendix B. ■

Remark 3: We define the depth of beam focusing range as the high correlation region of point (θ_0, ϕ_0, r_0), which shows the energy distribution of the beam that is fully targeted to the point (θ_0, ϕ_0, r_0). Lemma 4 provides two interesting insights into the impact of the far-field beams on the near-field EH, as described below.

- Note that if $\Gamma = 0.5$ and $\theta_0 = 0$, then $r_{\rm DF} = \frac{N^2 d^2}{2\lambda \eta_{\rm 3dB}^2} \approx \frac{D^2}{2\lambda \eta_{\rm 3dB}^2} \approx \frac{1}{10} R_{\rm ray}$. When $r_0 < r_{\rm DF}$, the boundaries of the high correlation region are precisely defined by $r_{\min}$ and $r_{\max}$. The energy of the beam directed toward the desired location (θ_0, ϕ_0, r_0) can be focused in the high correlation region. On the other hand, if $r_0 \geq r_{\rm DF}$, the upper bound of the high correlation region $r_{\max}$ approaches infinity, which means that the energy of the beam targeted to this area cannot be focused even if this area is in the near field. Therefore, the spherical wavefronts can only be exploited to generate focused beams in specific spatial region (i.e., $r_0 < r_{\rm DF}$).
- Taking $\Gamma = 0.5$ and $\theta_0 = 0$ as an example, it is observed that the expression of $r_{\min} = \frac{r_{\rm DF} r_0}{r_{\rm DF} + r_0}$ has the following characteristic. Assuming the desired location (θ_0, ϕ_0, r_0) is in the far field, i.e., $r_0 \geq 10 r_{\rm DF} = R_{\rm ray}$, we have $r_{\min} = \frac{10 r_{\rm DF}^2}{10 r_{\rm DF} + r_{\rm DF}} \approx 0.9 r_{\rm DF}$. This observation shows the fact that, even if a near-field receiver is from the same angle with a far-field beam, the channel correlation between the IR pointed by the far-field beam and the near-field receiver may be poor, and thus, the beam does not cause significant communication interference or strong energy supply to the receiver, especially when the distance between the receiver and the transmitter is small.

Based on the above discussion, we can give the lemma of distance beam-scheduling method.

Lemma 5: For MS $(\theta_k, \phi_k, r_k), \forall k \in \mathcal{K}_{\rm MS}$, if $\exists m \in \mathcal{M}_{\rm IR}$ satisfying $\theta_m = \theta_k$, $\phi_m = \phi_k$ and $r_k \geq r_{\min} = \frac{r_m r_{\rm DF}}{r_m + r_{\rm DF}}$, then the beam-scheduling matrix element of MS k can be given by $\alpha_k^{\rm E} = 0$, otherwise $\alpha_k^{\rm E} = 1$.

Proof: This lemma can be proved using the similar steps given in Appendix A. ■

Combining Lemma 1, Lemma 3, and Lemma 5, we have the following lemma for the beam-scheduling method for near-field MSs.

Lemma 6: For MS $(\theta_k, \phi_k, r_k), \forall k \in \mathcal{K}_{\rm MS}$, if $\exists m \in \mathcal{M}_{\rm IR}$ satisfying $\theta_k \in [\arcsin(\frac{-\theta_\Delta \lambda}{N\pi d \cos\phi_m} + \sin\theta_m), \arcsin(\frac{\theta_\Delta \lambda}{N\pi d \cos\phi_m} + \sin\theta_m)]$, $\phi_k \in [\arccos(\frac{\phi_\Delta \lambda}{N\pi d \sin\theta_m} + \cos\phi_m), \arccos(\frac{-\phi_\Delta \lambda}{N\pi d \sin\theta_m} + \cos\phi_m)]$, and $r_k \geq \frac{r_m r_{\rm DF}}{r_m + r_{\rm DF}}$, the beam-scheduling matrix element of MS k is given by $\alpha_k^{\rm E} = 0$; otherwise, we have $\alpha_k^{\rm E} = 1$.

C. Low-complexity Algorithm Design

Utilizing the results in Lemma 2 and Lemma 6, the beam-scheduling matrix elements of both far-field IRs and near-field MSs can be obtained as $\mathbf{A}^\star = \operatorname{diag}((\alpha_1^{\rm E})^\star, \ldots, (\alpha_K^{\rm E})^\star, (\alpha_1^{\rm I})^\star, \ldots, (\alpha_M^{\rm I})^\star)$. where $\{(\alpha_1^{\rm E})^\star, \ldots, (\alpha_K^{\rm E})^\star, (\alpha_1^{\rm I})^\star, \ldots, (\alpha_M^{\rm I})^\star\}$ is the beam-scheduling sequence obtained by Lemma 2 and Lemma 6. Then the problem (36) can be reduced to a power allocation problem, which can be solved by using iterations, as follows. At the $(q+1)$-th iteration, given an initial feasible point $\mathbf{P}^{(q)}$, we will get a power allocation problem, and then we again use WMMSE method to handle the non-convex sum-rate objective function. Specifically, the received signal of IR m is given by

$$\begin{aligned} y'_m = {} & n_m^{\rm I} + \sum_{k=1}^{K} (\alpha_k^{\rm E})^\star \sqrt{P_k^{\rm E} g_m^{\rm I}} |\boldsymbol{a}^H(\theta_m, \phi_m) \boldsymbol{b}(\theta_k, \phi_k, r_k)| x_k^{\rm E} \\ & + \sum_{i=1, i\neq m}^{M} (\alpha_i^{\rm I})^\star \sqrt{P_i^{\rm I} g_m^{\rm I}} \big|\boldsymbol{a}^H(\theta_m, \phi_m) \boldsymbol{a}(\theta_m, \phi_i)\big| x_i^{\rm I} \\ & + (\alpha_m^{\rm I})^\star \sqrt{P_m^{\rm I} g_m^{\rm I}} x_m^{\rm I}. \end{aligned} \tag{40}$$

By introducing equalizer $\tilde{u}_m$ and positive weight $\tilde{v}_m$, the estimation of the received signal y'_m can be expressed as $\tilde{y}'_m = \tilde{u}_m y'_m$ and the MSE for IR m can be given by

$$\begin{aligned} e'_m = {} & \mathbb{E}|y'_m - \tilde{y}'_m|^2 = |\tilde{u}_m|^2 \sigma_m^2 - 2\Re\{\tilde{u}_m (\alpha_m^{\rm I})^\star \sqrt{P_m^{\rm I} g_m^{\rm I}}\} \\ & + |\tilde{u}_m|^2 \sum_{i=1}^{M} \alpha_i^{\rm I} P_i^{\rm I} g_m^{\rm I} |\boldsymbol{a}^H(\theta_m, \phi_m) \boldsymbol{a}(\theta_i, \phi_i)|^2 \\ & + |\tilde{u}_m|^2 \sum_{k=1}^{K} \alpha_k^{\rm E} P_k^{\rm E} g_m^{\rm I} |\boldsymbol{a}^H(\theta_m, \phi_m) \boldsymbol{b}(\theta_k, \phi_k, r_k)|^2 + 1 \\ & \leq Y(m) + 1 - 2\Re\{\tilde{u}_m (\alpha_m^{\rm I})^\star \sqrt{g_m^{\rm I}}\} \bigg(\sqrt{(P_m^{\rm I})^{(q)}} \\ & + \frac{1}{2\sqrt{(P_m^{\rm I})^{(q)}}} \big(P_m^{\rm I} - (P_m^{\rm I})^{(q)}\big) \bigg) + |\tilde{u}_m|^2 \sigma_m^2 \triangleq \tilde{e}'_m, \end{aligned} \tag{41}$$

where $Y(m) \triangleq |\tilde{u}_m|^2 \sum_{i=1}^{M} \alpha_i^{\rm I} P_i^{\rm I} g_m^{\rm I} |\boldsymbol{a}^H(\theta_m, \phi_m) \boldsymbol{a}(\theta_i, \phi_i)|^2 + |\tilde{u}_m|^2 \sum_{k=1}^{K} \alpha_k^{\rm E} P_k^{\rm E} g_m^{\rm I} |\boldsymbol{a}^H(\theta_m, \phi_m) \boldsymbol{b}(\theta_k, \phi_k, r_k)|^2$, and $(P_m^{\rm I})^{(q)}$ is the power of IR m at q-th iteration. As such, problem (36) can be equivalently reformulated as

$$\min_{\mathbf{P}, \{v_m\}, \{u_m\}} \sum_{m=1}^{M} \tilde{v}_m \tilde{e}'_m - \log_2 |\tilde{v}_m| \tag{42a}$$

$$\begin{aligned} \text{s.t.} \quad & (36c), (36d) \\ & \log_2 |\tilde{v}_m| - \tilde{u}_m \tilde{e}'_m + 1 \geq R_{\min,m}, \\ & \forall m \in \mathcal{M}_{\rm IR}, \end{aligned} \tag{42b}$$

where the optimal value of $\tilde{v}_m$ and $\tilde{u}_m$ can be represented as

$$\tilde{v}_m^\star = 1 + \frac{(\alpha_m^{\rm I})^\star P_m^{\rm I} g_m^{\rm I}}{Y(m) \frac{1}{|\tilde{u}_m|^2} + \sigma_m^2}, \tilde{u}_m^\star = \frac{(\alpha_m^{\rm I})^\star \sqrt{P_m^{\rm I} g_m^{\rm I}}}{Y(m) \frac{1}{|\tilde{u}_m|^2} + \sigma_m^2}. \tag{43}$$

For the EH requirement constraint (36c), we use the same method in Section III-A and obtain the equivalent form as follows

$$\begin{aligned} & \sum_{i=1}^{K} \alpha_i^{\rm E} P_i^{\rm E} g_k^{\rm E} |\boldsymbol{b}^H(\theta_k, \phi_k, r_k) \boldsymbol{b}(\theta_i, \phi_i, r_i)|^2 + \sum_{m=1}^{M} \alpha_m^{\rm I} P_m^{\rm I} g_k^{\rm E} \\ & \times |\boldsymbol{b}^H(\theta_k, \phi_k, r_k) \boldsymbol{a}(\theta_m, \phi_m)|^2 \geq \bar{P}_k^{\rm in}(E_{\min,k}), \forall k \in \mathcal{K}_{\rm MS}, \end{aligned} \tag{44}$$

Algorithm 2 Low-complexity algorithm for Solving (12)

```
Initialize variable P^(0), iteration index q = 0, and threshold δ.
Fix beam direction with f̃_k^E = b(φ_k, r_k) and f̃_m^I = a(φ_m)
Obtain A through Lemma 2 and Lemma 5
repeat
    Update ṽ_m and ũ_m in (43).
    Update P^(q+1) by solving LP problem (45).
    q = q + 1.
until the fractional decrease of (45) is below δ, output P^(q+1)
Recover F_A and F_D by P^(q+1) F̃ = F_A F_D.
```

which is a linear constraint for the variable $\mathbf{P}$. Therefore, the problem can be rewritten as

$$\begin{aligned} \min_{\mathbf{P}} \ & \sum_{m=1}^{M} \tilde{v}_m \tilde{e}'_m - \log_2 |\tilde{v}_m| \\ \text{s.t.} \ & \text{(36d)}, \text{(42b)}, \text{(44)}. \end{aligned} \tag{45}$$

We observe that the objective function and the constraints in problem (45) are all affine. Thus, problem (45) is an LP problem, and can be solved using CVX successively until convergence. At last, the full digital beamforming $\mathbf{F}_{\mathrm{D}}$ and the analog beamforming $\mathbf{F}_{\mathrm{A}}$ are recovered by $\mathbf{P}\tilde{\mathbf{F}} = \mathbf{F}_{\mathrm{A}}\mathbf{F}_{\mathrm{D}}$. The overall low-complexity algorithm is summarized in Algorithm 2.

Since the beam scheduling matrix $\mathbf{A}$ is obtained by Lemma 6 of the revised manuscript, and the beam directions are fixed by $\tilde{\mathbf{f}}_k^{\mathrm{E}} = \boldsymbol{b}(\phi_k, r_k)$ and $\tilde{\mathbf{f}}_m^{\mathrm{I}} = \boldsymbol{a}(\phi_m)$, the convergence of the low-complexity algorithm relies on the convergence of the LP problem (45) based on the WMMSE method. Since the optimization result of the q-th iteration is used as the initial solution for the $(q+1)$-th iteration, a non-decreasing achievable sum rate can be obtained after $(q+1)$-th iteration. On the other hand, because the PS' transmit power is limited, the system has an upper bounded achievable sum rate. Hence, the low-complexity algorithm is guaranteed to converge. The computation complexity for solving problem (45) is obtained as $\mathcal{O}(I_{\mathrm{LP}}(K+M))$ [40], where I_{LP} is the number of iterations.

V. Simulation Results

Numerical results are used to validate the efficiency of two proposed algorithms. We consider a 3D network topology, as shown in Fig. 3, where the PS is located at the coordinate origin, serving at most 6 MSs and 6 IRs. Specifically, under the polar coordinates, the MSs 1 to 6 are located at (1.5708rad, 0, 30m), (1.043rad, 0.5256rad, 90m), (0.7854rad, $-$0.7854rad, 200m), (1.0472rad, $-$0.5256rad, 150m), (0.5256rad, 1.0472rad, 120m), and (0.7825rad, 0.788rad, 100m), respectively, while IRs 1 to 6 are located at (1.5708rad, 0, 700km), (1.0472rad, 0.5236rad, 710km), (0.7825rad, 0.7825rad, 720km), (1.0472rad, $-$0.5256rad, 710km), (0.7825rad, $-$0.3927rad, 720km), and (0.5256rad, $-$0.5256rad, 720km), respectively. Without loss of generality, in the following simulation, if we set $K=3$, then MS 1 to MS 3 will be in the satellite system to perform EH, while the remaining MS 4 to MS 6 will be reasonably ignored. If we set $K=6$, then all 6 MSs will perform EH. Similarly, if we set $M=4$, then IR 1 to IR 4 will communicate with the PS, and the remaining IR 5 to IR 6 can be ignored. Other parameters used in simulations are summarized in Table I.

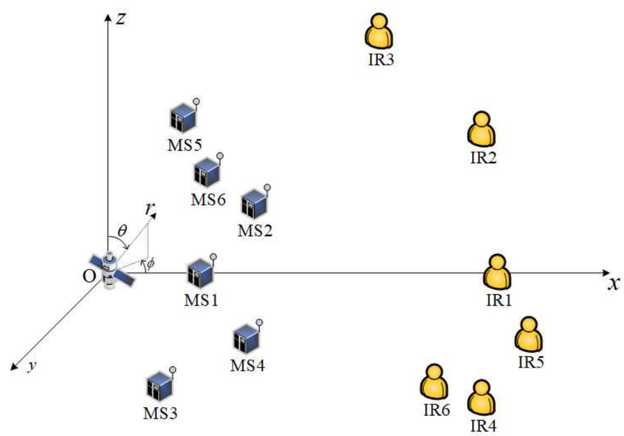

Fig. 3: Simulation setup for fractionated spacecraft enabled SWIPT system.

TABLE I: Simulation Parameters

Parameter	Value
Number of RF chain	$N_{\mathrm{RF}} = 2(K+M)$ [35]
Carrier frequency	$f = 100$ GHz [41]
Carrier wavelength	$\lambda = 0.003$ m [41]
Antenna spacing	$d = \frac{\lambda}{2} = 0.0015$ m [41]
EH circuit parameters	$j_k = 0.021$, $l_k = 20$, $\forall k$ [42]
Saturation power	$M_k = 100$ mW, $\forall k$ [42]
Maximum power budget	$P_{\max} = 40 \sim 50$ dBm [43]
Noise power	$\sigma_m^2 = -120$ dBm $\forall m$ [44]
Receiver antenna gain	$G_{\mathrm{R},k} = 40$ dBi $\forall k$ [45]

Remark 4: To perfectly approximate any full-digital beamforming design, the RF chains number of hybrid beamforming design has to be at least twice the number of receivers, i.e., $N_{\mathrm{RF}} \geq 2(K+M)$ [35]. Considering hardware costs and without loss of generality, we set $N_{\mathrm{RF}} = 2(K+M)$.

We compare with the following three benchmark schemes: **1) Algorithm in [23]:** This scheme adopts the same algorithm in [23] to obtain power allocation and beam-scheduling solution with fixed beamforming direction; **2) Low-complexity beam scheduling and equal power allocation (LC-EP):** This scheme adopts the low-complexity beam scheduling strategy in Lemma 6 and allocates equal power for all scheduled beams; **3) All beam scheduling and equal power allocation (ABS-EP):** In this scheme, each receiver (MS or IR) has a dedicated beam with equal power allocation.

In Fig. 4, we illustrate the convergence performance of the proposed algorithms. We set $K=M=3$, $P_{\max}=40$ dBm, $N=512$, $E_{\min,1}=E_{\min,2}=0.1$ mW, and $E_{\min,3}=0.01$ mW. It can be seen that the two proposed algorithms converge in 10 iterations. It can also be observed from Fig. 4 that the AO algorithm achieves a larger sum rate than the low-complexity algorithm, since the AO algorithm first allocates all the power to the information beams targeted to the IRs for maximizing

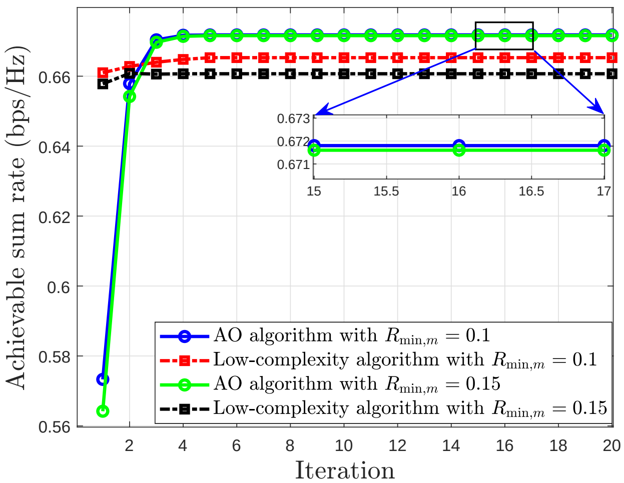

Fig. 4: Convergence behavior of the proposed algorithms.

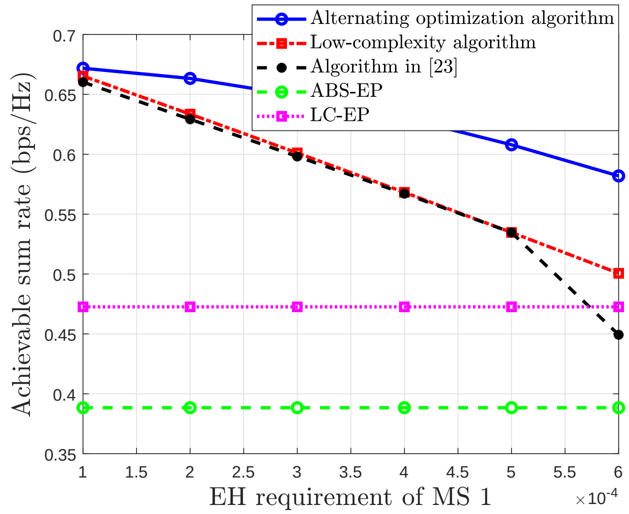

Fig. 6: Achievable sum rate versus EH requirement of MS 1.

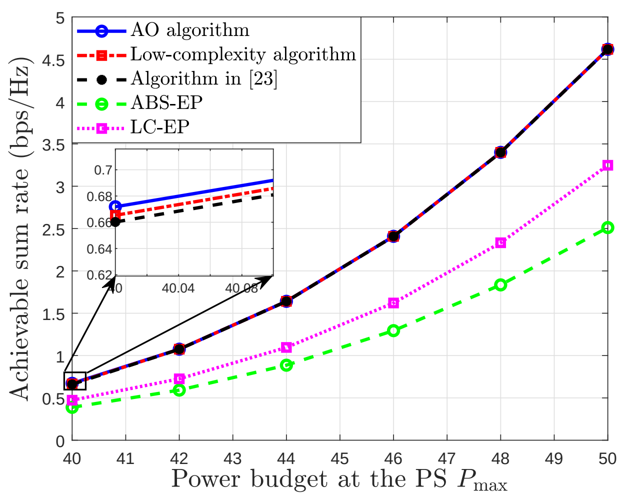

Fig. 5: Achievable sum rate versus PS's power budget $P_{\max}$.

the sum rate and then adjusts the directions of information beams to provide sufficient energy to MSs, which will not cause rate performance loss. In low-complexity algorithm, the beam is fixed to point at each receiver (i.e., $\tilde{\mathbf{f}}_k^{\mathrm{E}} = \boldsymbol{b}(\theta_k, \phi_k, r_k)$ and $\tilde{\mathbf{f}}_m^{\mathrm{I}} = \boldsymbol{a}(\theta_m, \phi_m)$), and the power allocated to the MSs cannot benefit the information transmission, resulting in rate loss. Moreover, Fig. 4 shows that the achievable sum rate of all algorithms decreases with $R_{\min,m}$. This is expected since a larger $R_{\min,m}$ indicates a more stringent QoS constraint, which renders each IR to fulfill its QoS requirement at the cost of increasing the transmit power allocated to the IRs with larger path loss, thus leading to a smaller sum rate.

Fig. 5 illustrates the impact of the PS's power budget on the system achievable sum rate. In this figure, we set $K = M = 3$, $R_{\min,m} = 0.1$ bps/Hz $\forall m$, $N = 512$, $E_{\min,1} = E_{\min,2} = 0.1$ mW, and $E_{\min,3} = 0.01$ mW. It is seen that a higher power budget leads to a high achievable sum rate for each scheme. Our two proposed algorithms have higher achievable sum rate than other schemes. The proposed AO algorithm has a higher achievable sum rate than the low-complexity algorithm when the power budget of the PS is small. But their performance gap almost shrinks to zero when the power budget is beyond $P_{\max} = 42$ dBm, due to the following reason. the two proposed algorithms almost achieve the same sum rate. The reason can be attributed to the following fact. Given the PS's small power budget, the AO algorithm can adjust its beam directions to adapt to information transmission and EH (i.e., with a flexibility of beamforming), and thus, can get a higher sum rate than low-complexity algorithm. When the PS has a large power budget, more energy from the information beams in low-complexity algorithm is sufficient for the MS's EH, thus the low-complexity algorithm can utilize more power for information transmission and achieve almost the same sum rate with the AO algorithm. From Fig. 5, the ABS-EP scheme has the worst performance, which demonstrates the importance of the beam scheduling and beamforming optimization on the system performance.

Fig. 6 plots the impact of one single MS's EH requirement on the system performance. Without loss of generality, we select MS 1 with $K = M = 3$, $P_{\max} = 40$ dBm, $R_{\min,m} = 0.1$ bps/Hz $\forall m$, $N = 512$, $E_{\min,2} = 0.1$ mW, and $E_{\min,3} = 0.01$ mW. From Fig. 6, the increase of MS 1's EH requirement is harmful to the achievable sum rate of the proposed algorithms. Indeed, a higher EH requirement causes extra power consumption at MS 1, leading to more resources being allocated to EH rather than information transmission, which is not beneficial for the enhancement of the rate performance. Moreover, the performance gap between AO algorithm and the low-complexity algorithm increases due to the flexible beamforming design in AO algorithm. Since the AO algorithm can adjust the power allocation and direction of the beams from the near angle of MS 1 to achieve energy supply, while the beam direction is fixed by $\tilde{\mathbf{f}}_k^{\mathrm{E}} = \boldsymbol{b}(\theta_k, \phi_k, r_k)$ and $\tilde{\mathbf{f}}_m^{\mathrm{I}} = \boldsymbol{a}(\theta_m, \phi_m)$ in low-complexity algorithm, and thus the increased EH requirement of MS 1 forces the low-complexity algorithm to allocate more power for the dedicated energy beam, resulting in a significant decrease of achievable sum

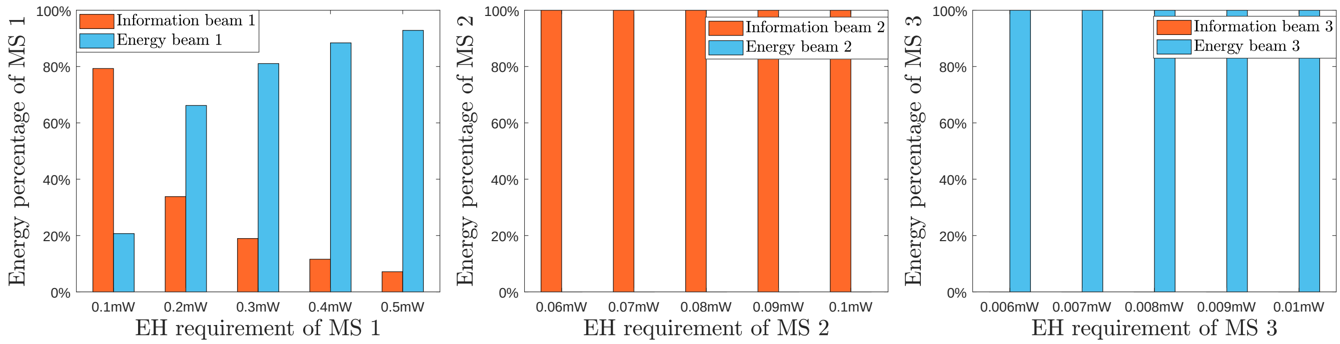

(a) MS 1.

(b) MS 2.

(c) MS 3.

Fig. 7: Energy Percentage for each MS from all information and energy beams versus each MS's EH requirement.

rate. It can also be observed from Fig. 6 that the achievable sum rate of ABS-EP and LC-EP schemes remain unchanged with the increase of MS 1's EH requirement, because of the resource allocation strategy with equal power allocation.

For each MS, Fig. 7 shows the percentage of energy it harvests from information beams and percentage of energy it harvests from energy beams, where the information beam m is the information-bearing beam scheduled for IR m, and the energy beam k is the energy-bearing beam scheduled for MS k. In this figure, we set $K = M = 3$, $P_{\max} = 40$ dBm, $R_{\min,m} = 0.1$ bps/Hz $\forall m$, and $N = 512$. It is observed from Fig. 7(a)–(c) that MS 1 can harvest energy not only from information beam 1, but also from the energy beam 1, while the energy demand of MS 2 can be satisfied by information beam 2 only, and the EH requirement of MS 3 is fully achieved by its dedicated energy beam 3. These observations can be explained as follows. Since the PS equipped with a large-scale antenna array can achieve far-field high-directivity beam steering and near-field beam focusing, MS k can harvest energy from both far-field information beams pointing to near its angle and the dedicated energy beam scheduled for MS k. First, MS 1 is from the same angle with IR 1, indicating that MS 1 is able to harvest enough energy from the information beam 1 to sustain its functionality, as discussed in Remark 2. However, the distance between MS 1 and the PS does not satisfy the condition in Lemma 6, and thus a dedicated energy-bearing beam must be scheduled for MS 1. For MS 2, although it is not from an exact same angle with IR 2, both the angle θ_2, ϕ_2 and distance r_2 of MS 2 satisfy the conditions in Lemma 6. Therefore, the energy required by MS 2 is all provided by the far-field information beam 2 from the similar angle. On the other hand, there is no IR from the angle of MS 3, and hence the energy beam 3 must be scheduled for its energy supply. From Fig. 7(a), it is also observed that the harvested energy percentage of MS 1 from energy beam 1 increases as the EH requirement of MS 1 increases. This suggests that with a large EH requirement, the near-field MS 1 cannot harvest sufficient energy from the far-field beams in the same angle, which forces the PS to schedule energy beam 1 to support its functionality. The reason for this phenomenon is that the channel coherence between MS 1 and IR 1 is poor, and the wireless energy received by MS 1 from information beam 1 is largely reduced, leading to more power allocated to energy beams for energy supply. This implies that, different from the existing beam-scheduling strategy in [23], where the energy beam must be scheduled for near-field EH receivers, it is preferable to utilize far-field information beams to satisfy near-field EH requirement unless there are no information beams for IR which is from the near angle of the near-field EH receivers or the EH demand of the energy receivers is very large.

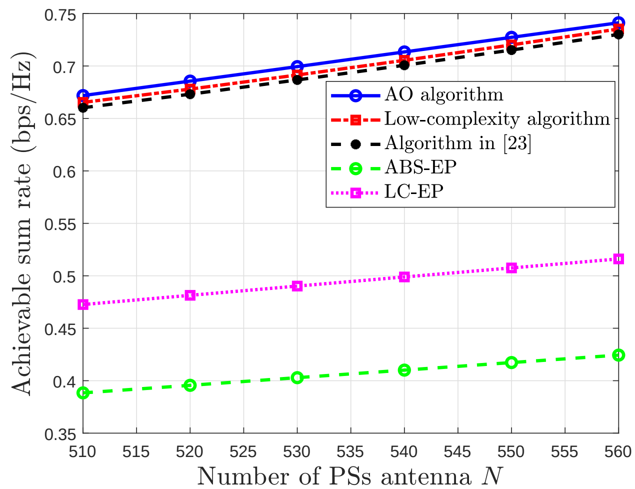

Fig. 8: Achievable sum rate versus the number of PS's antennas.

Fig. 8 depicts the achievable sum rate of the overall system versus the number of PS's antennas, where $K = M = 3$, $P_{\max} = 40$ dBm, $R_{\min,m} = 0.1$ bps/Hz $\forall m$, $E_{\min,1} = E_{\min,2} = 0.1$ mW, and $E_{\min,3} = 0.01$ mW. More antennas at the PS result in higher achievable sum rate for all the schemes. Our two proposed algorithms perform much better than other benchmark schemes.

Fig. 9 shows achievable sum rate versus the number of IRs, where $K = 3$, $P_{\max} = 50$ dBm, $N = 512$, $R_{\min,m} = 0.1$ bps/Hz $\forall m$, $E_{\min,1} = E_{\min,2} = 0.1$ mW, and $E_{\min,3} = 0.01$ mW. It can be seen from the figure that the achievable sum rate achieved by all the algorithms increases with the increased number of IRs. The phenomenon is because that the PS can

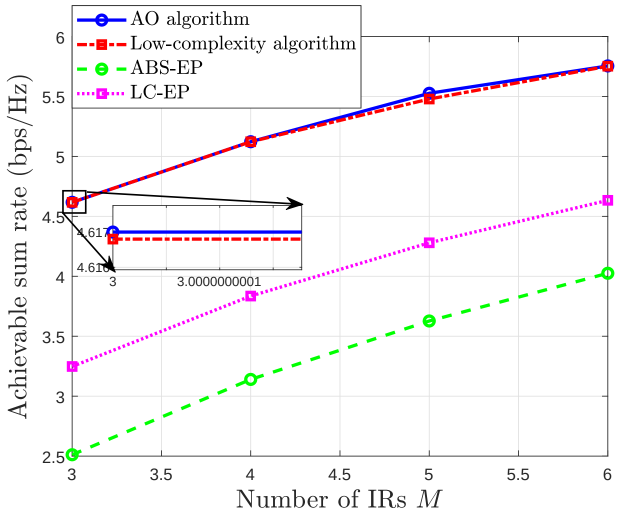

Fig. 9: Achievable sum rate versus the number of IRs.

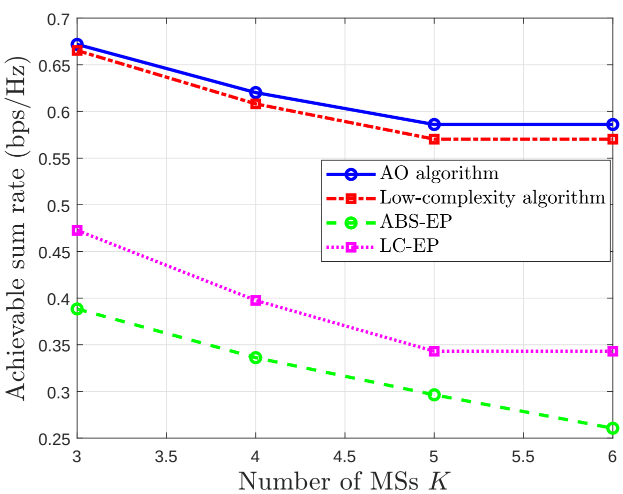

Fig. 10: Achievable sum rate versus the number of MSs.

effectively mitigate inter-user interference through beamforming. In this context, each additional IR contributes its own rate without significantly degrading other IRs' performance.

Fig. 10 shows the achievable sum rate performance when the number of MSs varies, where $M = 3$, $P_{\max} = 40$ dBm, $N = 512$, $R_{\min,m} = 0.1$ bps/Hz $\forall m$, $E_{\min,1} = E_{\min,2} = 0.1$ mW, and $E_{\min,3} = E_{\min,4} = E_{\min,5} = E_{\min,6} = 0.01$ mW. We can observe from the figure that as the number of MSs increases, the achievable sum rate of all the algorithms decreases. The reason behind this behavior is that there is no any information beam near MS 4 and MS 5, which forces the PS to allocate power to achieve the energy requirement of MS 4 and MS 5, leading to a reduced rate performance. Fortunately, there is a dedicated information beam 3 for IR 3 near MS 6, and thus the addition of MS 6 will not affect the rate performance of the satellite system.

VI. Conclusion and Future Works

In this paper, we studied a SWIPT-enabled fractionated spacecraft system and formulated an optimization problem to maximize the achievable sum rate of the IRs by jointly designing the digital/analog beamforming and beam scheduling matrix, subject to the EH constraints of MSs. An AO algorithm was then developed to solve the formulated problem based on the WMMSE method, MO method, and matching theory. By utilizing the intrinsic structure of mixed near- and far-field for fractionated spacecraft system, the coherence between near- and far-field steering vectors was derived and a low-complexity algorithm was proposed to solve the formulated sum rate maximization problem by exploiting the characteristics of the coherence. We provided simulation results to demonstrate the efficiency of our proposed algorithms. Furthermore, unlike existing mixed near- and far-field SWIPT systems in ground scenarios, it is wise to utilize far-field information beams to achieve energy supply for near-field energy receivers in fractionated spacecraft systems.

We conclude the paper with some potential extensions of the proposed SWIPT-enabled fractionated spacecraft system and future research directions as follows. First, in this paper we consider that all the MSs are in the near-field of the PS and they only harvest energy from the PS. In some scenarios, MSs also receive necessary mission information from the PS. Therefore, it is necessary to consider the MSs' EH and communication requirements simultaneously, and design effective operating protocols for MSs, which deserves further investigation. Second, the energy source of the PS has not been considered in this paper. In practical systems, the PS needs to convert the Sun's energy into electricity to support energy supply and information transmission for MSs and IRs. In this scenario, it is meaningful to design an operation protocol and transmission scheme for an energy-limited multi-functional PS to improve energy efficiency. Last but not the least, in this paper, we assume that only a single fractionated spacecraft system communicates with the ground IRs. In more general scenarios, multiple fractionated spacecraft systems may communicate with the ground IRs simultaneously, and information transmission is also required between the multiple fractionated spacecraft systems. As a result, the MSs are able to harvest energy not only from space-to-ground communication signals, but also from inter-satellite communication signals. In this context, it will be interesting to investigate beamforming and beam-scheduling design for multi-satellite space-to-ground SWIPT.

Appendix A
Proof of Lemma 1

If $\exists m \in \mathcal{M}_{\text{IR}}$ satisfies $\phi_k \in [\arccos(\frac{\phi_\Delta \lambda}{N\pi d \sin\theta_m} + \cos\phi_m), \arccos(\frac{-\phi_\Delta \lambda}{N\pi d \sin\theta_m} + \cos\phi_m)]$, at least one of IR's steering vector has a strong correlation with MS k, i.e., the value of $|\boldsymbol{b}^H(\theta_k, \phi_k, r_k)\boldsymbol{a}(\theta_m, \phi_m)|^2$ is large. This indicates that at least one of the third terms on the right side of equation (34) is large enough to guarantee that MS k harvests enough energy to power its operation. Thus, the PS does not need to transmit a dedicated energy-bearing beam for MS k, i.e., $\alpha_k = 0$. Otherwise, only the first term on the right side of equation (34) is large enough to provide energy for MS k, which forces $\alpha_k = 1$. This thus proves Lemma 1.

APPENDIX B
PROOF OF LEMMA 3

For arbitrary two locations (θ_0, ϕ_0, r_0) and (θ_0, ϕ_0, r) from the same azimuth and elevation angles, the coherence of their steering vectors can be expressed as

$$\begin{aligned} f(\theta_1, \theta_2, \phi_1, \phi_2, r_1, r_2) &= f(\theta_0, \theta_0, \phi_0, \phi_0, r_0, r) \\ &= \left| \frac{1}{N} \sum_{n=(N-1)/2}^{(N-1)/2} e^{j\pi n^2 \frac{d^2(1-\sin^2\theta_0\cos^2\phi_0)}{\lambda}(\frac{1}{r_0}-\frac{1}{r})} \right| \\ &\triangleq |F(x)|, \end{aligned} \tag{46}$$

where $x = \frac{d^2(1-\sin^2\theta_0\cos^2\phi_0)}{\lambda}(\frac{1}{r_0}-\frac{1}{r})$, and the function $F(x)$ is given by

$$F(x) = \frac{1}{N} \sum_{n=(N-1)/2}^{(N-1)/2} e^{j\pi n^2 x} \approx \frac{1}{N} \int_{-N/2}^{N/2} e^{j\pi n^2 x} dn. \tag{47}$$

If $r_0 \leq r$, then $x = \frac{d^2(1-\sin^2\theta_0\cos^2\phi_0)}{\lambda}(\frac{1}{r_0}-\frac{1}{r}) \geq 0$. Letting $n^2 x = \frac{1}{2}t^2$, we have

$$\begin{aligned} F(x) &= \frac{2}{\sqrt{2x}N} \int_0^{\sqrt{2x}N/2} e^{j\frac{\pi}{2}t^2} dt \\ &= \frac{\int_0^{\sqrt{2x}N/2} \cos(\frac{\pi}{2}t^2)dt + j\int_0^{\sqrt{2x}N/2} \sin(\frac{\pi}{2}t^2)dt}{\sqrt{2x}N/2}. \end{aligned} \tag{48}$$

It is obvious that $\int_0^{\sqrt{2x}N/2} \cos(\frac{\pi}{2}t^2)dt$ and $\int_0^{\sqrt{2x}N/2} \sin(\frac{\pi}{2}t^2)dt$ are Fresnel functions. Denote $\beta = \frac{\sqrt{2x}N}{2} = \sqrt{\frac{N^2 d^2(1-\sin^2\theta_0\cos^2\phi_0)}{2\lambda}(\frac{1}{r_0}-\frac{1}{r})}$, $C(\beta) = \int_0^{\sqrt{2x}N/2} \cos(\frac{\pi}{2}t^2)dt$, and $S(\beta) = \int_0^{\sqrt{2x}N/2} \sin(\frac{\pi}{2}t^2)dt$, the function $F(x)$ can be rewritten as

$$F(x) = \frac{C(\beta) + jS(\beta)}{\beta} = T(\beta). \tag{49}$$

Moreover, if $r_0 > r$, then we have $-x = \frac{d^2(1-\sin^2\theta_0\cos^2\phi_0)}{\lambda}(\frac{1}{r_0}-\frac{1}{r}) > 0$. Similar to the derivation of (49), if $-x > 0$, then $F(x) = T^\dagger(\beta)$, where $\beta = \frac{\sqrt{2x}N}{2} = \sqrt{\frac{N^2 d^2(1-\sin^2\theta_0\cos^2\phi_0)}{2\lambda}(\frac{1}{r}-\frac{1}{r_0})}$. In summary, the coherence can be approximated as $f(\theta_0, \theta_0, \phi_0, \phi_0, r_0, r) = |F(x)| \approx |T(\beta)|$, where $\beta \approx \sqrt{\frac{N^2 d^2(1-\sin^2\theta_0\cos^2\phi_0)}{2\lambda}\left|\frac{1}{r_0}-\frac{1}{r}\right|}$. Substituting the approximate expression of the coherence $f(\theta_0, \theta_0, \phi_0, \phi_0, r_0, r) \approx |T(\beta)|$ and $\Gamma = 0.5$ into the inequality $f(\theta_0, \theta_0, \phi_0, \phi_0, r_0, r) \geq \Gamma$, we have $|T(\beta)| \geq 0.5$. According to the numerical result of $T(\beta)$ [39], we can obtain $\beta \leq \eta_{3\text{dB}} = 1.6$, i.e., $\sqrt{\frac{N^2 d^2(1-\sin^2\theta_0\cos^2\phi_0)}{2\lambda}\left|\frac{1}{r_0}-\frac{1}{r}\right|} \leq \eta_{3\text{dB}}$, which is equivalent to $\max\left\{0, \frac{1}{r_0} - \frac{2\lambda\eta_{3\text{dB}}^2}{N^2 d^2(1-\sin^2\theta_0\cos^2\phi_0)}\right\} \leq \frac{1}{r} \leq \frac{1}{r_0} + \frac{2\lambda\eta_{3\text{dB}}^2}{N^2 d^2(1-\sin^2\theta_0\cos^2\phi_0)}$. Recall $r_{\text{DF}} = \frac{N^2 d^2(1-\sin^2\theta_0\cos^2\phi_0)}{2\lambda\eta_{3\text{dB}}^2}$, if $r_0 < r_{\text{DF}}$, the range of r can be obtained as $\frac{r_{\text{DF}}r_0}{r_{\text{DF}}+r_0} \leq r \leq \frac{r_{\text{DF}}r_0}{r_{\text{DF}}-r_0}$. Thus, the depth of beam focusing is given by $\Xi = \frac{r_{\text{DF}}r_0}{r_{\text{DF}}-r_0} - \frac{r_{\text{DF}}r_0}{r_{\text{DF}}+r_0} = \frac{2r_0^2 r_{\text{DF}}}{r_{\text{DF}}^2 - r_0^2}$. If $r \geq r_{\text{DF}}$, the range of r is given by $\frac{r_{\text{DF}}r_0}{r_{\text{DF}}+r_0} \leq r \leq \infty$, and the depth of beam focusing is given by $\Xi = \infty$. This completes the proof.

REFERENCES

[1] O. Brown and P. Eremenko, "Fractionated space architectures: A vision for responsive space," in *Proc. of 4th Responsive Space Conf.*, pp. 1–6, 2006.

[2] C. Mathiew and A. Weigel, "Assessing the flexibility provided by fractionated spacecraft," *Space* 2005, pp. 6700, 2005.

[3] C. Mathiew and A. Weigel, "Assessing the fractionated spacecraft concept," *Space* 2006, pp. 7212, 2006.

[4] M. A. Koets *et al.*, "Enabling fractionated spacecraft communications using F6WICS," in *MILCOM 2012-2012 IEEE Military Commun. Conf.*, pp. 1–5, 2012.

[5] A. Dubey *et al.*, "A software platform for fractionated spacecraft," in *Proc. IEEE Aerosp. Conf.*, pp. 1–5, 2012.

[6] J. Guo, DC Maessen, and E. Gill, "Fractionated spacecraft: The new sprout in distributed space systems," in *58th International Astronautical Congress*, 2009.

[7] J. Chu, J. Guo, and E. Gill, "Functional, physical, and organizational architectures of a fractionated space infrastructure for long-term earth observation missions," *IEEE Trans. Aerosp. Electron. Syst.*, vol. 29, no. 12, pp. 6–17, Dec. 2014.

[8] L. Chi, F. Sun, Z. Liu, and C. Lin, "Overview of fractionated spacecraft technology," in 2020 *International Conf. on Computer Engineering and Application (ICCEA)*, IEEE, 2020, pp. 689–692.

[9] I. Krikidis *et al.*, "Simultaneous wireless information and power transfer in modern communication systems," *IEEE Commun. Mag.*, vol. 52, no. 11, pp. 104–110, Nov. 2014.

[10] X. Lu *et al.*, "Wireless networks with RF energy harvesting: A contemporary survey," *IEEE Commun. Surveys Tuts.*, vol. 17, no. 2, pp. 757–789, 2nd Quart., 2015.

[11] G. Pan *et al.*, "Simultaneous lightwave information and power transfer: Policies, techniques, and future directions," *IEEE Access*, vol. 7, pp. 28250–28257, Feb. 2019.

[12] J. Lafleur and J. Saleh, "GT-FAST: A point design tool for rapid fractionated spacecraft sizing and synthesis," in *AIAA Space* 2009 *Conf. and Exposition*, pp. 6563, 2009.

[13] J. Lafleur and J. Saleh, "System-level feasibility assessment of microwave power beaming for small satellites," *J. of Propulsion and Power*, vol. 25, no. 4, pp. 976–983, 2009.

[14] V. Jamnejad and A. Sliva, "Microwave power beaming strategies for fractionated spacecraft systems," in *IEEE Aerospace Conf.*, 2008.

[15] G. Pan *et al.*, "Space simultaneous information and power transfer: An enhanced technology for miniaturized satellite systems," *IEEE Wireless Commun.*, vol. 30, no. 2, pp. 122–129, Apr. 2023.

[16] A. Alfadreek, A. Roula, I. Otung, and L. Uggalla, "Massive phased array antenna with ±50° beam steering for space communications at W-band frequency," *IET Conf. Proc. CP879*, vol. 2024, no. 4, pp. 36–41, 2024.

[17] H. Zhang, *et al.*, "6G wireless communications: From far-field beam steering to near-field beam focusing," *IEEE Commun. Mag.*, vol. 61, no. 4, pp. 72–77, Apr. 2023.

[18] K. Huang, L. You, M. Qian, and X. Gao, "MetaSWIPT: DMA-assisted multi-user MISO downlink simultaneous wireless information and power transfer," *IEEE Wireless Commun. Lett.*, vol. 13, no. 4, pp. 1048–1052, Jan. 2024.

[19] N. Song and H. Dai, "Optimal beam-focusing design for 6G near-field SWIPT systems," *IEICE Commun. Exp.*, vol. 13, no. 3, pp. 84–87, Mar. 2024.

[20] Z. Zhang, *et al.*, "Simultaneous wireless information and power transfer in near-field communications," *IEEE Internet Things J.*, vol. 11, no. 16, pp. 27760–27774, Aug. 2024.

[21] H. Chen, *et al.*, "STAR-RIS assisted hybrid far- and near-field SWIPT," *IEEE Trans. Veh. Technol.*, early access, Aug. 29, 2025, doi: 10.1109/TVT.2025.3603715.

[22] Y. Yi, *et al.*, "AN-aided secure beamforming for ELAA-SWIPT in mixed near- and far-field," *IEEE Wireless Commun. Lett.*, early access, Sep. 2025, doi: 10.1109/LWC.2025.3605106.

[23] Y. Zhang and C. You, "SWIPT in mixed near- and far-field channels: Joint beam scheduling and power allocation," *IEEE J. Sel. Areas Commun.*, vol. 42, no. 6, pp. 1583–1597, Apr. 2024.

[24] Y. Zhang, C. You, L. Chen, and B. Zheng, "Mixed near- and far-field communications for extremely large-scale array: An interference perspective," *IEEE Commun. Lett.*, vol. 27, no. 9, pp. 2496–2500, Sep. 2023.

[25] Y. Liu *et al.*, "Near-field communications: A tutorial review," *IEEE Open J. Commun. Soc.*, vol. 4, pp. 1999–2049, 2023.

[26] M. Cui *et al.*, "Near-field MIMO communications for 6G: Fundamentals, challenges, potentials, and future directions," *IEEE Commun. Mag.*, vol. 61,, no. 1, pp. 40–46, Jan. 2023.
[27] E. Björnson, Ö. T. Demir, and L. Sanguinetti, "A primer on near-field beamforming for arrays and reconfigurable intelligent surfaces," in *Proc.* 55*th Asilomar Conf. Signals, Syst., Comput.*, Oct. 2017, pp. 105–112.
[28] M. Gao, S. Zhu, S. Xu, and J. Dai, "Weighted sum rate maximization for cell free massive MIMO network of LEO satellite," *IEEE Trans. Veh. Technol.*, early access, Mar. 2026, doi: 10.1109/TVT.2026.3669895.
[29] X. Wang *et al.*, "Joint Bayesian channel estimation and data detection for OTFS systems in LEO satellite communications" *IEEE Trans. Commun.*, vol. 70, no. 4, pp. 4386–4399, July 2022.
[30] B. Zheng, S. Lin, and R. Zhang, "Intelligent reflecting surface-aided LEO satellite communication: Cooperative passive beamforming and distributed channel estimation," *IEEE J. Sel. Areas Commun.*, vol. 38, no. 8, pp. 1719–1734, Oct. 2020.
[31] J. Lin, Y. Tian, D. Liu, and Z. Zhang, "Time-varying channel estimation for LEO satellite communications with millimeter wave massive MIMO," *IEEE Sensors J.*, vol. 25, no. 20, pp. 39159–39172, Oct. 2025.
[32] E. Boshkovska, D. W. K. Ng, N. Zlatanov, and R. Schober, "Practical non-linear energy harvesting model and resource allocation for SWIPT systems," *IEEE Commun. Lett.*, vol. 19, no. 12, pp. 2082–2085, Dec. 2015.
[33] J. Liu, G. Yang, Y. Liu, and X. Zhou, "RIS empowered near-field covert communications," *IEEE Trans. Wireless Commun.*, vol. 23, no. 10, pp. 15477–15492, Oct. 2024.
[34] Q. Shi, M. Razaviyayn, Z.-Q. Luo, and C. He, "An iteratively weighted MMSE approach to distributed sum-utility maximization for a MIMO interfering broadcast channel," *IEEE Trans. Signal Process.*, vol. 59, no. 9, pp. 4331–4340, Sep. 2011.
[35] F. Sohrabi and W. Yu, "Hybrid digital and analog beamforming design for large-scale antenna arrays," *IEEE J. Sel. Topics Signal Process.*, vol. 10, no. 3, pp. 501–513, Apr. 2016.
[36] K. Bando, "Many-to-one matching markets with externalities among firms," *J. Math. Econ.*, vol. 48, no. 1, pp. 14–20, Jan. 2012.
[37] C. Pan *et al.*, "Intelligent reflecting surface aided MIMO broadcasting for simultaneous wireless information and power transfer," *IEEE J. Sel. Areas Commun.*, vol. 38, no. 8, pp. 1719–1734, Aug. 2020.
[38] H. Guo, Y.-C. Liang, J. Chen, and E. G. Larsson, "Weighted sum-rate maximization for reconfigurable intelligent surface aided wireless networks," *IEEE Trans. Wireless Commun.*, vol. 19, no. 5, pp. 3064–3076, May 2020.
[39] M. Cui and L. Dai, "Channel estimation for extremely large-scale MIMO: Far-field or near-field?" *IEEE Trans. Commun.*, vol. 70, no. 4, pp. 2663–2677, Jan. 2022.
[40] L. Lv *et al.*, "RIS-assisted wireless powered MEC: Multiple access design and resource allocation," *IEEE Trans. Wireless Commun.*, vol. 24, no. 2, pp. 984–1000, Feb. 2025.
[41] Y. Xing and T. S. Rappaport, "Terahertz wireless communications: Co-sharing for terrestrial and satellite systems above 100 GHz," *IEEE Commun. Lett.*, vol. 25, no. 10, pp. 3156–3160, Oct. 2021.
[42] R. Jiang *et al.*, "Optimal design of SWIPT systems with multiple heterogeneous users under non-linear energy harvesting model," *IEEE Access*, vol. 5, pp. 11479–11489, Jun. 2020.
[43] Z. Xiang *et al.*, "Decoupled precoder and receiver design for massive MIMO multiple LEO satellite communication," *IEEE Trans. Wireless Commun.*, vol. 25, pp. 9747–9764, 2026.
[44] J. Wang *et al.*, "Joint antenna positioning and beamforming for movable antenna array aided ground station in low-earth orbit satellite communication," *IEEE Trans. Wireless Commun.*, vol. 25, pp. 9437–9451, 2026.
[45] M. Takahashi *et al.*, "Adaptive power resource allocation with multi-beam directivity control in high-throughput satellite communication systems," *IEEE Wireless Commun. Lett.*, vol. 8, no. 4, pp. 1248–1251, Aug. 2019.

Long Yang (Senior Member, IEEE) received the B.E. and Ph.D. degrees from Xidian University, Xi'an, China, in 2010 and 2015, respectively. Since December 2015, he has been a Faculty Member with Xidian University, where he is currently a Full Professor with the State Key Laboratory of Integrated Services Networks. From September 2016 to December 2016, he was a Visiting Researcher with the School of Computing and Communications, Lancaster University, Lancaster, U.K. From November 2017 to October 2019, he was a Post-Doctoral Fellow with the Department of Electrical and Computer Engineering, University of Alberta, Edmonton, Canada. His current research interests include non-orthogonal multiple access, mobile-edge computing, covert communications and flexible antennas. He was a Leading Guest Editor of IEEE INTERNET OF THINGS JOURNAL on Special Issue Ultra-Reliable and Low-Latency Satellite Communications for Ubiquitous Internet of Everything (IoE). He is currently serving as an Associate Editor for IEEE TRANSACTIONS ON VEHICULAR TECHNOLOGY, IEEE COMMUNICATIONS LETTERS, and IET Communications.

Hao Luo received the B.Eng. degree from Xidian University, China, in 2022, where he is currently pursuing the Ph.D degree. His current research interests include reconfigurable intelligent surface, non-orthogonal multiple access, physical layer security, and movable antenna.

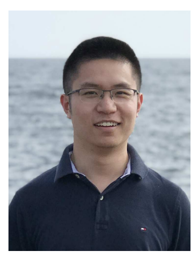

Lu Lv (Member, IEEE) received the Ph.D. degree from Xidian University, China, in 2018. From 2016 to 2018, he was an Academic Visitor with Lancaster University and the University of Alberta. In 2019, he was a Post-Doctoral Fellow with Dalhousie University. He is currently an Associate Professor with Xidian University. His research interests include non-orthogonal multiple access, reconfigurable intelligent surface, and covert communication. He was a recipient of the Outstanding Ph.D. Thesis Award of Shaanxi Province in 2020, the IEEE ICCC Best Paper Award in 2021, and the Exemplary Reviewer Certificate for IEEE TRANSACTIONS ON COMMUNICATIONS from 2018 to 2020 and IEEE COMMUNICATIONS LETTERS in 2022. He was listed as a Worlds Top 2% Scientist by Stanford University from 2022 to 2024. He is serving as an Associate Editor for IEEE INTERNET OF THINGS JOURNAL, IEEE OPEN JOURNAL OF THE COMMUNICATIONS SOCIETY, and *Frontiers in Computer Science*.

Yuchen Zhou received the B.Eng. and Ph.D. degrees from Xidian University, Xi'an, China, in 2013 and 2018, respectively. She was a joint Ph.D. Student with Carleton University, Ottawa, ON, Canada, from 2016 to 2018. In 2018, she joined the School of Telecommunications Engineering, Xidian University, where she is currently an Associate Professor. Her current research interests include the Internet-of-Things, cyber-physical systems, machine learning, and wireless network virtualization.

Xuan Xue (Member, IEEE) received the B.E. and Ph.D. degrees from Xidian University, Xian, China, in 2010 and 2017, respectively. From 2013 to 2015, she was a Visiting Ph.D. Student with Western University, London, ON, Canada. Since 2018, she has been a Faculty Member with Xidian University, where she is currently an Associate Professor with the School of Telecommunications Engineering, Xidian University. Her research interests include massive MIMO, millimeter-wave communications, cooperative communications, and non-orthogonal multiple access.

Xiaoli Chu (Senior Member, IEEE) received the B.Eng. degree in electronic and information engineering from Xian Jiaotong University, China, in 2001, and the Ph.D. degree in electrical and electronic engineering from The Hong Kong University of Science and Technology in 2005. From 2005 to 2012, she was with the Centre for Telecommunications Research, Kings College London, U.K. She is currently a Professor with the School of Electrical and Electronic Engineering, The University of Sheffield, U.K. She has co-authored over 200 peer-reviewed journals and conference papers, including eight ESI Highly Cited Papers and the IEEE Communications Society 2017 Young Author Best Paper. She has co-authored/co-edited four books: *Fog-Enabled Intelligent IoT Systems* (Springer 2020), *Ultra Dense Networks for 5G and Beyond* (Wiley 2019), *Heterogeneous Cellular Networks-Theory, Simulation and Deployment* (Cambridge University Press 2013), and *4G Femtocells: Resource Allocation and Interference Management* (Springer 2013). She received the Best Performing Editor Award of the IEEE Vehicular Technology Society in 2024, the 2024 Exemplary Editor Award from IEEE TRANSACTIONS ON MACHINE LEARNING IN COMMUNICATIONS AND NETWORKING, and IEEE Communications Letters Exemplary Editor Award in 2018. She is an Editor of IEEE TRANSACTIONS ON WIRELESS COMMUNICATIONS, IEEE TRANSACTIONS ON NETWORK SCIENCE AND ENGINEERING, and IEEE TRANSACTIONS ON MACHINE LEARNING IN COMMUNICATIONS AND NETWORKING

Hai Jiang (Fellow, IEEE) received the B.Sc. and M.Sc. degrees in electronics engineering from Peking University, Beijing, China, in 1995 and 1998, respectively, and the Ph.D. degree in electrical engineering from the University of Waterloo, Waterloo, ON, Canada, in 2006. Since 2007, he has been a Faculty Member with the University of Alberta, Edmonton, AB, Canada, where he is currently a Professor with the Department of Electrical and Computer Engineering. His research interests include radio resource management, mobile edge computing, and cooperative communications.